Functional genomics of cattle through integration of multi-omics data

Hamid Beiki[1], Brenda M. Murdoch[2], Carissa A. Park[1], Chandlar Kern[3], Denise Kontechy[2], Gabrielle Becker[2], Gonzalo Rincon[4], Honglin Jiang[5], Huaijun Zhou[6], Jacob Thorne[2], James E. Koltes[1], Jennifer J. Michal[7], Kimberly Davenport[2], Monique Rijnkels[8], Pablo J. Ross[6], Rui Hu[5], Sarah Corum[4], Stephanie McKay[9], Timothy P.L. Smith[10], Wansheng Liu[3], Wenzhi Ma[3], Xiaohui Zhang[7], Xiaoqing Xu[6], Xuelei Han[7], Zhihua Jiang[7], Zhi-Liang Hu[1], James M. Reecy[1]

[1]Department of Animal Science, Iowa State University; [2]Department of Animal and Veterinary and Food Science, University of Idaho; [3]Department of Animal Science, Pennsylvania State University; [4]Zoetis; [5]Department of Animal and Poultry Sciences, Virginia Tech; [6]Department of Animal Science, University of California, Davis; [7]Department of Animal Science, Washington State University; [8]Department of Veterinary Integrative Biosciences, Texas A&M University; [9]University of Vermont; [10]USDA, ARS, USMARC.

Corresponding author:

James M. Reecy

Professor of Animal Breeding and Genetics, Department of Animal Science, Ames, IA, USA

jreecy@iastate.edu

Abstract

Functional annotation of the bovine genome was performed by characterizing the spectrum of RNA transcription using a multi-omics approach, combining long- and short-read transcript sequencing and orthogonal data to identify promoters and enhancers and to determine boundaries of open chromatin. A total number of 171,985 unique transcripts (50% protein-coding) representing 35,150 unique genes (64% protein-coding) were identified across tissues. Among them, 159,033 transcripts (92% of the total) were structurally validated by independent datasets such as PacBio Iso-seq, ONT-seq, *de novo* assembled transcripts from RNA-seq, or Ensembl and NCBI gene sets. In addition, all transcripts were supported by extensive independent data from different technologies such as WTTS-seq, RAMPAGE, ChIP-seq, and ATAC-seq. A large proportion of identified transcripts (69%) were novel, of which 87% were produced by known genes and 13% by novel genes. A median of two 5' untranslated regions was detected per gene, an increase from Ensembl and NCBI annotations (single). Around 50% of protein-coding genes in each tissue were bifunctional and transcribed both coding and noncoding isoforms. Furthermore, we identified 3,744 genes that functioned as non-coding genes in fetal tissues, but as protein coding genes in adult tissues. Our new bovine genome annotation extended more than 11,000 known gene borders compared to Ensembl or NCBI annotations. The resulting bovine transcriptome was integrated with publicly available QTL data to study tissue-tissue interconnection involved in different traits and construct the first bovine trait similarity network. These validated results show significant improvement over current bovine genome annotations.

Introduction

Domestic bovine (*Bos taurus*) provides a valuable source of nutrition and an important disease model for humans (Roth and Tuggle 2015). Furthermore, cattle have the greatest number of genotype associations and genetic correlations of the domesticated livestock species, which means they provide an excellent model to close the genotype-to-phenotype gap. Therefore, the accurate identification of the functional elements in the bovine genome is a fundamental requirement for high quality analysis of data informing both genome biology and clinical genomics.

Current annotations of farm animal genomes largely focus on the protein-coding regions and fall short of explaining the biology of many important traits that are controlled at the transcriptional level (Beiki et al. 2019). In humans, 88% of trait-associated single nucleotide polymorphisms (SNP) identified by genome-wide association studies (GWAS) are found in non-coding regions (Hindorff et al. 2009). Therefore, elucidating non-coding functional elements of the genome is essential for understanding the mechanisms that control complex biological processes.

Untranslated regions play critical roles in the regulation of mRNA stability, translation, and localization (Jereb et al. 2018), but these regions have been poorly annotated in farm animals (Schurch et al. 2014; Beiki et al. 2019). A recent study of the pig transcriptome using single-molecule long-read isoform sequencing technology resulted in the extension of more than 6000 known gene borders compared to Ensembl or National Center for Biotechnology Information (NCBI) annotations (Beiki et al. 2019).

Small non-coding RNAs, such as microRNAs (miRNA), are known to be involved in gene regulation through post-transcriptional regulation of expression via silencing, degradation, or sequestering to inhibit translation (Ambros 2004; Bartel 2004; Yates et al. 2013). The number of annotated miRNAs in the current bovine genome annotation (Ensembl release 2018-11; 951 miRNAs) is much lower than the number reported in the highly annotated human genome (Ensembl release 2021-03; 1,877 miRNAs).

This study applied a comprehensive set of transcriptome and chromatin state data from 47 cattle tissues and cell types to identify previously unannotated genes and improve the annotation of thousands of protein-coding and non-coding genes. Predicted novel genes and transcripts were highly supported by independent Pacific Biosciences single-molecule long-read isoform sequencing (PacBio Iso-Seq), Oxford Nanopore Technologies sequencing (ONT-seq), Illumina high-throughput RNA sequencing (RNA-seq), Whole Transcriptome Termini Site Sequencing (WTTS-seq), RNA Annotation and Mapping of Promoters for the Analysis of Gene Expression (RAMPAGE), chromatin immunoprecipitation sequencing (ChIP-seq), and Assay for Transposase-Accessible Chromatin using sequencing (ATAC-seq) data. The transcriptome data was integrated with publicly available Quantitative Trait Loci (QTL) and gene association data to construct the first bovine trait similarity network that recapitulates published genetic correlations. Thus, it may be possible to begin to examine the genetic mechanisms underlying genetic correlations.

Results

The diversity of RNA and miRNA transcript diversity among 47 different bovine tissues and cell types was assessed using miRNA-seq and poly(A)-selected RNA-seq and miRNA-seq data. Most of the tissues studied were from Hereford cattle closely related to L1 Dominette 01449, the individual from which the bovine reference genome (ARS-UCD1.2) was sequenced. The 47 tissues and cell samples included follicular cells, myoblasts, five mammary gland samples from various stages of mammary gland development and lactation, eight fetal tissues (78-days of gestation), eight tissues from adult digestive tract, and 16 other adult organs. A total of approximately 4.1 trillion RNA-seq reads and 1.2 billion miRNA-seq reads were collected, with a minimum of 27.5 million RNA-seq and 9.3 million miRNA-seq reads from each tissue/cell type (average 87.8 ± 49.7 million and 27.6 ± 12.9 million, respectively) (Supplemental file 1: Fig. S1 and Supplemental file 2).

Transcript level analyses

A total of 171,985 unique transcripts (76% spliced) were identified (Table 1) with a median of 51,231 transcripts per tissue. The median length of exons was 137 nt, and that of introns was 1,428 nt. Exonic length of transcripts (region of transcript covered by exons after collapsing transcript exons) was significantly longer (p-value < 2.2e-16) in spliced transcripts (median of 1,651 nt) compared to unspliced transcripts (median of 513 nt). There was a median of 9.1 exons per spliced transcript, and all of the predicted acceptor and donor splice sites conformed to the canonical consensus sequences. All of the predicted splice junctions across tissues were

supported by RNA-seq reads that spanned the splice junction, substantiating the accuracy of the transcript definition from RNA-seq reads.

Table 1. Summary of detected transcripts/genes

Feature	Annotation[1]		
	Cattle FAANG	Ensembl (Release 2021-03)	NCBI (Release 106)
Number of genes	35,150 (21,193)	27,607 (21,880)	35,143 (21,355)
Number of transcripts	171,985 (85,658)	43,984 (37,538)	83,195 (47,280)
Number of spliced transcripts	130,531	37,299	73,423
Number of transcripts per gene	4.9	1.5	2.3
Median number of 5' UTRs per gene	2	1	1
Median number of 3' UTRs per gene	1	1	1

[1]Numbers in parentheses indicate the number of protein-coding genes/transcripts.

A total of 31,476 transcripts appeared tissue-specific by virtue of being assembled from RNA-seq reads in just a single tissue, but 20,100 of those transcripts (64%) were actually expressed in multiple tissues according to long-read Iso-seq data. Thus, reliance solely on assembled transcripts in a given tissue to predict a tissue transcript atlas may overestimate tissue

110 specificity due to a high false-negative rate for transcript detection. To solve this problem of
111 over-prediction of tissue specificity, we marked a transcript as "detected" in a given tissue only
112 if (1) it had been assembled by RNA-seq data in that tissue; or (2) it had been detected by Iso-
113 seq data in another tissue, but all splice junctions were validated using RNA-seq reads in the
114 tissue of interest with an expression level more than 1 RPKM (see Methods section). This
115 resulted in 15,562 apparently tissue-specific transcripts (9%) and 156,423 transcripts (91%)
116 detected in more than one tissue (Fig. 1A), among which 9,125 transcripts (5%) were found in
117 all 47 tissues examined.

118

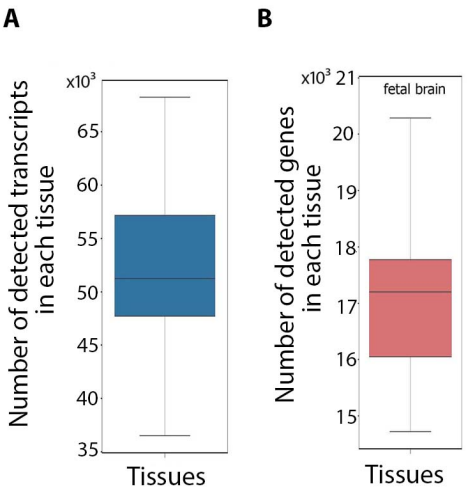

119

120 **Figure 1.** Distribution of the number of detected transcripts (A) and genes (B) across tissues.

121 The unique transcripts identified were equally distributed between 85,658 (50%) protein-
122 coding transcripts and 86,327 (50%) non-coding transcripts (ncRNAs) (Fig. 2). Non-coding
123 transcripts were further classified as long non-coding (lnc) RNAs (56%), nonsense-mediated
124 decay (NMD) transcripts (38%), non-stop decay (NSD) transcripts (5%), and small nuclear (sn)

RNAs (1%). While the majority of detected transcripts in each tissue were protein coding (median of 62% of tissue transcripts), NMD transcripts (median of 14.58% of tissue transcripts) and antisense lncRNAs (median of 12% of tissue transcripts) each made up more than 10% of the transcripts (Supplemental file 1: Fig. S2A and B, Supplemental file 3 and 4). Fetal muscle and fetal gonad tissues showed the highest proportion of antisense lncRNAs compared to that observed in other tissues (Supplemental file 1: Fig. S2B) and around 60% of antisense lncRNAs (17,982 transcripts) were detected from these two tissues. Compared to non-coding transcripts, protein-coding transcripts were more likely to have spliced exons (p-value < 2.2e-16) and were detected in a higher number of tissues (median of 11 tissues for protein-coding transcripts versus six tissues for non-coding transcripts; p-value < 2.2e-16) (Additional file1: Fig. S2C). The lncRNAs had a significantly lower splice rate (36%) compared to other non-coding transcripts (p-value < 2.2e-16). Splice rate was highest (70%) in sncRNAs (p-value < 2.2e-16; NMD transcripts were not included in this analysis, as they were all spliced transcripts by definition).

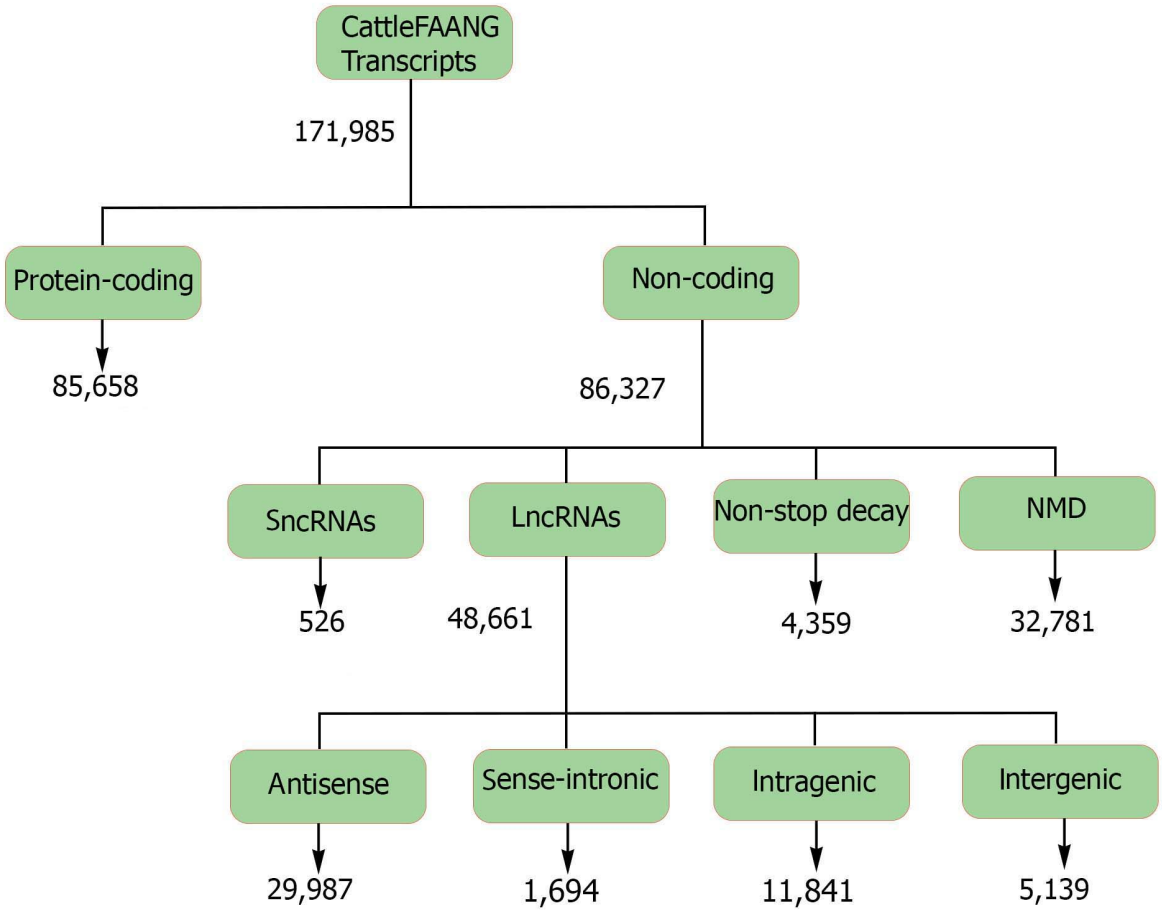

Figure 2. Classification of the predicted transcripts into different biotypes.

There were no significant correlations between the number of RNA-seq reads for a given tissue and the number of unique transcripts identified, except for a modest correlation for the antisense lncRNA class (Supplemental file 1: Fig. S3A). There was a significant positive correlation (p-value 1.3e-04) between the number of unique NMD transcripts in a tissue and the number of protein-coding transcripts, and the NMD transcript class showed the lowest median expression level across tissues, followed by antisense-lncRNAs and sense intronic-lncRNAs (Supplemental file 1: Fig. S2D and Fig. S3B). In addition, there was a significant positive

149 correlation (p-value 3.4e-03) between the number of NMD transcripts and the number of
150 protein-coding transcripts across tissues (Supplemental file 1: Fig. S3A). The expression levels of
151 sncRNAs and protein-coding transcripts were higher (p-values: 1.1e-02 and 2.6e-06,
152 respectively) than that observed for other transcript biotypes (Supplemental file 1: Fig. S2D and
153 Fig. S3B).

154 **Transcript similarity to other species**

155 Protein/peptide homology analysis of transcripts with coding potential (protein-coding
156 transcripts, lncRNAs, and sncRNAs) revealed a higher conservation rate of protein-coding
157 transcripts (86%) compared to lncRNA and sncRNA transcripts (8%; p-value < 2.2e-16) (Table 2).
158 Bovine non-coding transcripts had significantly (p-value < 2.2e-16) less similarity to other species
159 than protein-coding transcripts (Table 2 and Table 3). Within non-coding transcripts, NSD
160 transcripts showed the lowest conservation rate (35%), followed by sncRNAs (37%), lncRNAs
161 (49%), and NMD transcripts (55%), while sense intronic lncRNAs had the highest conservation
162 rate (60%) compared to other non-coding transcripts (Table 4).

163

164

165

166

167

Table 2. Protein/peptide homology of transcripts with coding potential

Transcript biotype	Number of transcripts	Transcripts with protein/peptide homology to other species[1]
Protein-coding transcripts	85,658	73,268 (86%)
sncRNAs and lncRNAs that encode short peptides[2]	48,425	4,054 (8%)

[1]Number in parentheses indicates the percentage of each transcript biotype.

[2]Open reading frame of 9 to 43 amino acids

168

Table 3. Sequence homology of non-coding transcripts

Transcript biotype	Number of transcripts	Transcripts with sequence homology to ncRNAs in other species[1]
Long non-coding RNAs	48,661	23,707 (49%)
Small non-coding RNAs	526	194 (37%)
Non-stop decay RNAs	4,359	1,551 (35%)
Nonsense-mediated decay RNAs	32,781	18,195 (55%)

[1]Number in parentheses indicates the percentage of each transcript biotype.

169

170

Table4. Sequence homology of different types of lncRNAs

lncRNA biotype	Number of transcripts	Transcripts with sequence homology to ncRNAs in other species[1]
antisense lncRNAs	29,987	13,793 (46%)
sense-intronic lncRNAs	1,694	1,029 (60%)
intragenic lncRNAs	5,569	2,314 (41%)
intergenic lncRNAs	11,841	5,820 (49%)

[1]Number in parentheses indicates the percentage of each transcript biotype.

171

172 **Transcript diversity across tissues**

173 A median of 70% of protein-coding transcripts were shared between pairs of tissues
174 (Supplemental file 1: Fig. S4A), significantly higher than that was observed for non-coding
175 transcripts (53%; p-value < 2.2e-16; Supplemental file 1: Fig. S5). Clustering of tissues based on
176 protein-coding transcripts was different than that observed based on non-coding transcripts
177 (Supplemental file 1: Fig. S4B and Fig. S5B, Fig. S35F). The fetal tissues clustered together and

were generally more similar to one another than to the corresponding adult tissue in both dendrograms, but thymus was closely related to fetal tissues for protein-coding transcript content, while it appeared more similar to lymph nodes, myoblasts, and pregnant/lactating mammary tissue using non-coding transcript profiles. The digestive tract tissues clustered together in the non-coding dendrogram with ileum as a slight outlier, while both jejunum and ileum were distant from the other digestive tissues in the protein-coding transcript profile. The "adult mammary gland" (78 day pregnant) and "virgin mammary gland" samples did not cluster with the three other pregnant/lactating mammary samples nor with each other in either dendrogram. This is mostly likely because: 1) these are from different physiological stages, 2) these were whole tissue samples while the other three pregnant/lactating samples are enriched for mammary gland epithelial cells, 3) the virgin and 78 day pregnant samples are from Hereford background while other pregnant/lactating samples are from Holstein-Frisian breed.

Fetal tissues had significantly higher proportions than adult tissues of unique non-coding transcripts (specifically NSDs, antisense lncRNAs, and intragenic lncRNAs) compared to protein-coding transcripts (p-value < 2.2e-16; Supplemental file 5).

Transcript validation

Prediction of transcripts and isoforms from RNA-seq data may produce erroneous predicted isoforms. The validity of transcripts was therefore examined by comparison to a library of isoforms taken from Ensembl and NCBI gene sets, plus an assembly produced from all RNA-seq reads, as well as isoforms identified through complete isoform sequencing with Pacific Biosciences and Oxford Nanopore platforms. A total of 118,563 transcripts (70% of predicted

199 transcripts) were structurally validated by at least one other independent dataset. A total of
200 160,610 transcripts were detected in multiple tissues (96% of predicted transcripts), providing
201 further support for their validity (Fig. 3). All transcripts were also extensively supported by
202 independent data from different technologies such as WTTS-seq, RAMPAGE, histone
203 modification (H3K4me3, H3K4me1, H3K27ac and CTCF), and ATAC-seq (Fig. 3).

204

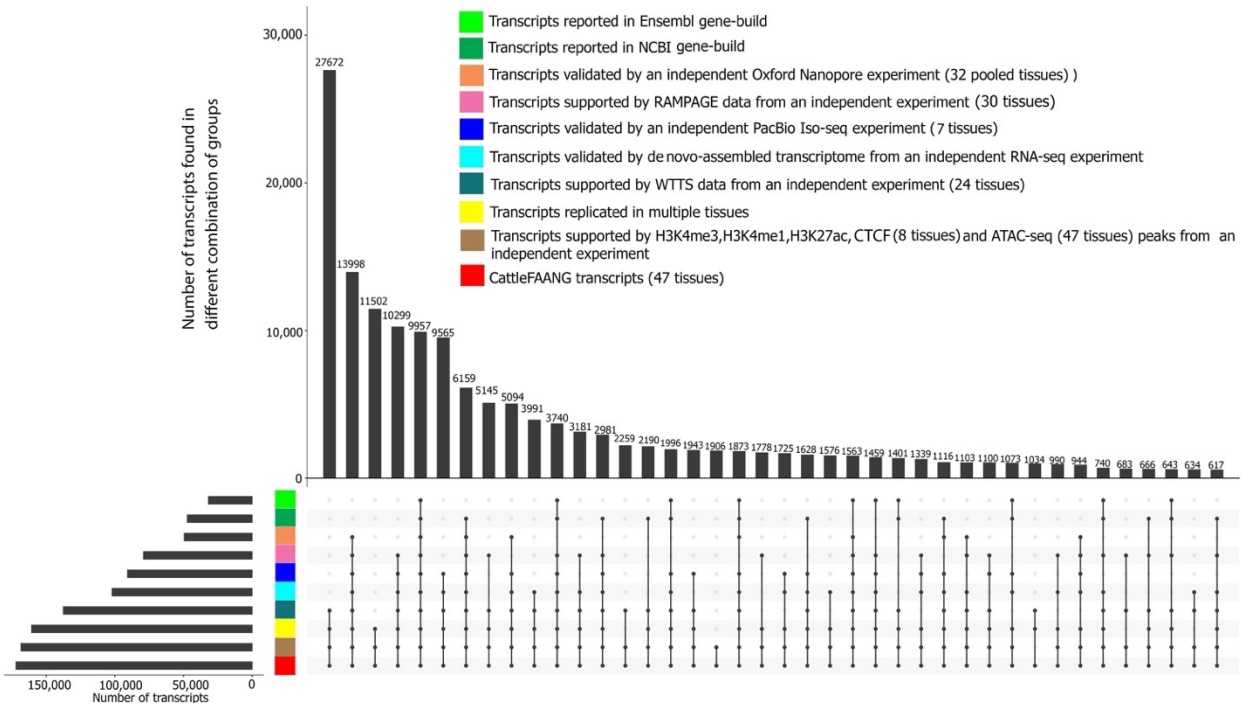

205

206

207 **Figure 3.** Validation of predicted transcripts using independent data from different
208 technologies.

209

Comparison of predicted transcript structures with known transcripts in the current bovine genome annotations (Ensembl release 2021-03 and NCBI Release 106) resulted in a total of 52,645 annotated transcripts that exactly matched previously annotated transcripts (31% of all transcripts), including 47,054 annotated NCBI transcripts, 31,740 annotated Ensembl transcripts, and 26,149 transcripts that were common to both annotated gene sets (Fig. 3). The median expression level of known transcripts in their detected tissues (1.8 RPKM) was similar to that observed for novel transcripts (1.4 RPKM) (Supplemental file 1: Fig. S6). Known transcripts were detected in a median of 17 tissues, which was higher (p-value 7.4e-03) than that observed for novel transcripts (median of seven tissues) (Supplemental file 1: Fig. S6). In addition, compared to novel transcripts, annotated transcripts were enriched with protein-coding (p-value 1.37e-02) and spliced transcripts (p-value 3.76e-02).

The median length of coding sequence (CDS) of known transcripts was 1,014 nt, significantly longer than that observed in novel transcripts (510 nt; p-value 0.0) (Additional file1: Fig. S7A). In addition, novel transcripts had longer 5’ UTRs (400 nt) compared to that was observed in known transcripts (300 nt, p-value 2.631E-06; Additional file1: Fig. S7A). Novel transcripts encoding proteins with homology to proteins annotated in other species had longer CDS (687 nt) compared to transcripts without such homology (192 nt; p-value 0.0). Known protein-coding transcripts showed a higher GC content in their 5’ UTRs (61%) than novel transcripts (53%; p-value 5.562E-18), but both classes of transcripts showed similar GC content within their CDS (Supplemental file 1: Fig. S7B).

Gene level analyses

The transcripts correspond to a total of 35,150 genes, which were detected and classified into protein coding (21,193), non-coding (10,928), and pseudogenes (3,029) (Supplemental file 3 and 4, Fig. 1B, and Fig. 4). The majority of genes detected in each tissue were protein coding (median of 83% of tissue genes), followed by non-coding (median of 14% of tissue genes) and pseudogenes (median of 3% of tissue genes) (Supplemental file 1: Fig. S8). Testis showed the highest number of detected genes with observed transcripts compared to other tissues (Supplemental file 1: Fig. S8). Fetal brain and fetal muscle tissues showed the highest number and percentage of non-coding genes compared to that observed in other tissues (Supplemental file 1: Fig. S8). In addition, more than 40% of transcripts corresponded to non-coding genes (1,271 genes) in fetal brain and fetal muscle. The proportion (6%) and number (1,271) of transcript-producing pseudogenes was higher in testis than in other tissues. There was no significant correlation between the number of input reads and the number of detected genes across tissues, but the numbers of genes from different coding potential classes were significantly correlated across tissues (Supplemental file 1: Fig. S9).

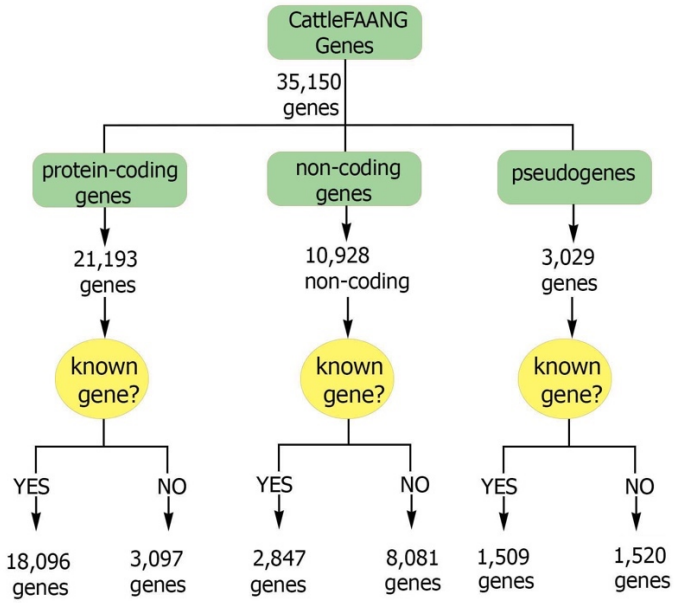

246

247 **Figure 4.** Classification of the predicted genes into different biotypes.

248 Transcripts corresponding to the predicted genes that had at least one exon overlapping an
249 Ensembl- or NCBI-annotated gene were considered to belong to a known gene. This supported
250 an intersection analysis of predicted and previously annotated genes that indicated 22,452
251 (64%) of our predicted genes correspond to previously known genes. Approximately 87% of
252 novel transcripts (103,387) were associated with this set of known genes. The remaining 12,698
253 genes (36% of predicted genes) represent novel genes, i.e., genes not found on Ensembl
254 (release 2021-03) or NCBI (release 106), with which 15% of novel transcripts (22,364
255 transcripts) were associated. The median number of unique transcripts per known gene (tpg)
256 was four, which was higher than that observed in either the Ensembl (1.5 tpg) or NCBI (2.3 tpg)
257 annotated gene sets, while the median number of transcripts per novel gene was one, with an
258 average of 1.31 and standard deviation of 1.36. Most of the transcripts identified were
259 transcribed from known genes, including 96% of protein-coding transcripts (82,060), 79% of

lncRNA transcripts (38,662), 78% of sncRNA transcripts (413), and more than 95% of NMD transcripts (31,422). Known genes were enriched with protein-coding genes (p-value < 2.2e-16). The median transcript abundance from known genes in their detected tissues (6.59 RPKM) was significantly higher than that observed for novel genes (median of 1.68 RPKM; p-value < 2.2e-16; Supplemental file 1: Fig. S10A). The median number of tissues in which known genes were detected (42 tissues) was also significantly higher than that observed for novel genes (median of four tissues; p-value < 2.2e-16; Supplemental file 1: Fig. S10B).

More than a third (37%) of genes with at least one predicted protein-coding transcript displayed either multiple 5' untranslated regions (UTRs) or multiple 3' UTRs (median of three 5' UTRs and three 3' UTRs per gene) among associated transcript isoforms (Fig. 5). The 496 genes with the highest number of UTRs (the top 5% in this metric) were highly enriched (q-value 1.7E-7) for the "response to protozoan" Biological Process (BP) Gene Ontology (GO) term (Supplemental file 1: Fig. S11 and Supplemental file 6).

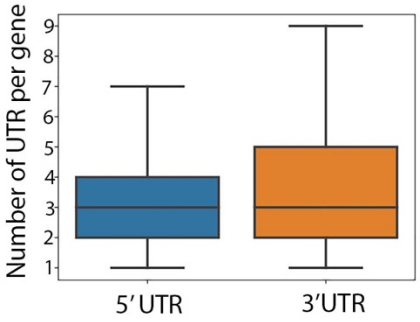

Figure 5. Distribution of the number of 5' UTRs and 3' UTRs per gene in genes with multiple UTRs.

A median of 51% of the detected protein-coding genes in each tissue transcribed both protein-coding and non-coding transcripts and were denoted as bifunctional genes. These genes were mostly previously annotated (95%) and had both coding and non-coding transcripts in a median of 21 tissues, representing 57% of their detected tissues (Fig. 6A and B). Protein-coding transcripts and NMD transcripts covered more than 90% of the exonic length in bifunctional genes (Fig. 6C). This percentage was significantly lower for other types of non-coding transcripts transcribed from bifunctional genes (77%, 81%, and 62% for NSD transcripts, sncRNAs, and intragenic lncRNAs, respectively) (Fig. 6C). Although transcript terminal sites (TTS) of transcripts encoded by bifunctional genes were centralized around these genes' 3' ends, transcript start sites (TSS) varied greatly among transcript biotypes (Fig. 6C). The TTSs of NSD transcripts, sncRNAs, and intragenic lncRNAs were shifted from their protein-coding genes' start sites (Fig. 6C). Genes that transcribed both protein-coding and non-coding transcripts in all of their detected tissues (1,661 genes) were highly enriched for "mRNA processing" (q-value 6.08E-16) and "RNA splicing" (q-value 1.35E-14) BP GO terms that were mostly (65%) related to different aspects of transcription and translation (Fig. 6D and Supplemental file 7).

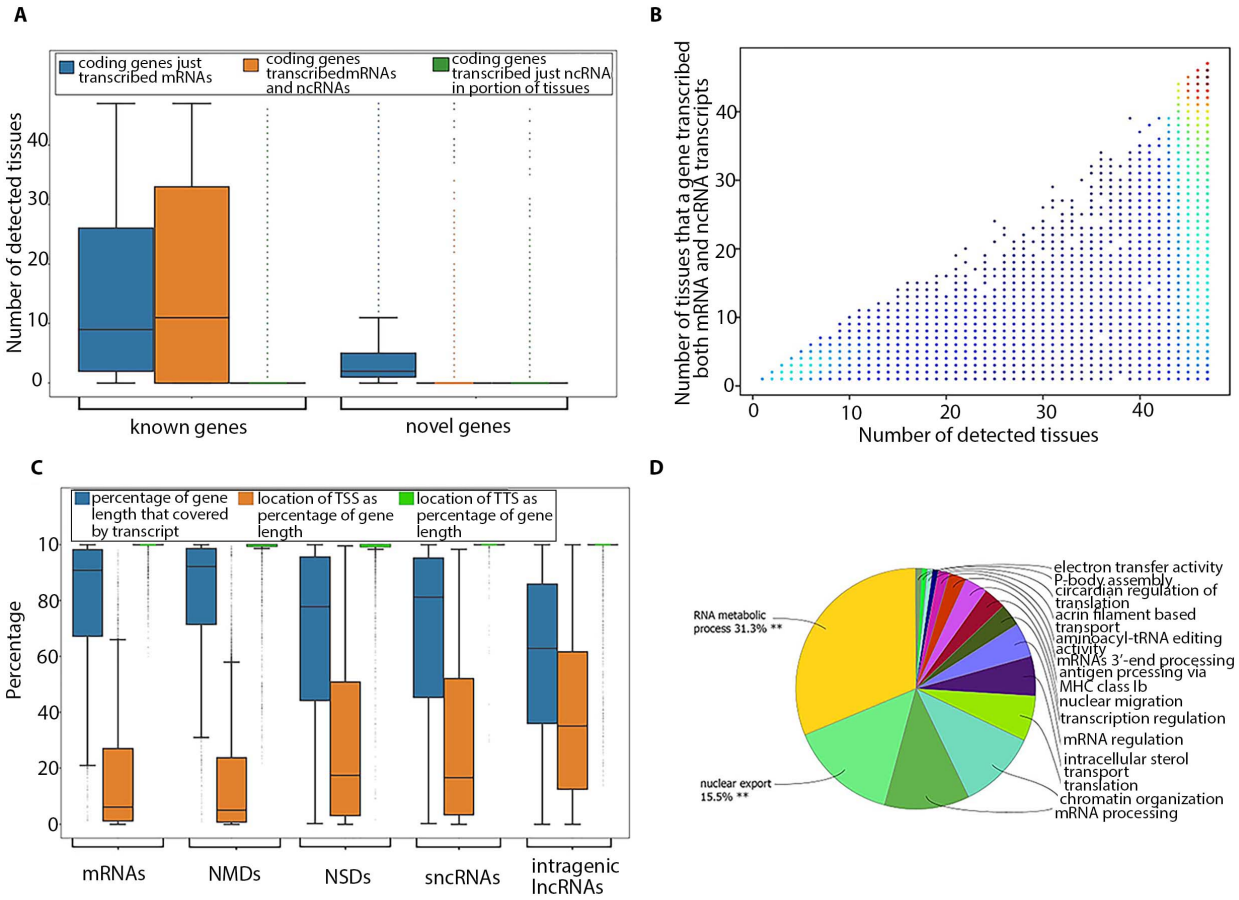

293

294 **Figure 6.** (A) Classification of protein-coding genes based on their novelty and types of encoded

295 transcripts. (B) Number of detected tissues for bifunctional genes. Dots have been color coded

296 based on their density. (C) Location of different transcript biotypes on bifunctional genes. (D)

297 Functional enrichment analysis of genes that remained bifunctional in all of their detected

298 tissues.

299

300 A total of 3,744 protein-coding genes (17% of all predicted protein-coding genes) only

301 transcribed non-coding transcripts in a median of two tissues (equivalent to 15% of their

302 detected tissues). Detailed investigation of these genes in tissues from both adult and fetal

303 samples (brain, kidney, muscle, and spleen) revealed the total of 106 non-coding genes (90%
304 known) in fetal tissues that were switched to protein-coding genes with only protein-coding
305 transcripts in their matched adult tissues (Supplemental file 1: Fig. S12). Functional enrichment
306 analysis of these genes resulted in the identification of enriched BP GO terms related to
307 “humoral immune response”, “sphingolipid biosynthetic process”, “negative regulation of
308 wound healing”, “cellular senescence”, “symporter activity”, “regulation of lipid biosynthetic
309 process”, and “filopodium assembly” (Supplemental file 1: Fig. S12, Supplemental file 8).

310 A median of 32% of protein-coding genes in each tissue expressed at least a single potentially
311 aberrant transcript (PAT), i.e., NMDs and NSDs. In this group of genes, the number of PATs was
312 strongly correlated with the total number of transcripts (median correlation of 0.61 across all
313 tissues). The median expression level of these genes in their detected tissues (11.52 RPKM) was
314 significantly higher (p-value < 2.2e-16) than for protein-coding genes with no PATs (4.48 RPKM).
315 In each tissue, protein-coding genes with PATs showed a significantly higher number of introns
316 (p-value < 2.2e-16; median of 65 introns per gene) than that observed in the remainder of
317 protein-coding genes (median of 15 introns per gene). In addition, genes from this group were
318 detected in a median of 47 tissues, significantly higher (p-value < 2.2e-16) than that observed
319 for the other coding genes (median of 24 tissues), non-coding genes (median of five tissues),
320 and pseudogenes (median of four tissues) (Supplemental file 1: Fig. S13A and B). These genes
321 transcribed a median of two PATs in half (median 54%) of their detected tissues, equivalent to a
322 median of 22% of all their transcripts in each tissue. Protein-coding genes that transcribed PATs
323 as their main transcripts (PATs comprised >50% of their transcripts) in all of their detected
324 tissues were highly enriched with RNA splicing–related BP GO terms (Supplemental file 9).

Gene similarity to other species

Eighty-five percent of protein-coding genes (18,087) encoded either homologous proteins (17,150 genes or 80% of protein-coding genes) or homologous ncRNAs (7,347 genes or 35% of protein-coding genes) (Supplemental file 1: Fig. S14A). Nineteen percent of protein-coding genes (4,043) encoded cattle-specific proteins (Supplemental file 1: Fig. S14A). The majority of these genes (2,750 or 68%) were either known genes or genes with homology to another cattle gene(s) that has established homology to genes in other species (Supplemental file 1: Fig. S14C). The remaining 32% of cattle-specific, protein-coding genes (1,293 genes or six percent of protein-coding genes) were denoted as protein-coding orphan genes (Supplemental file 1: Fig. S14C). A median of 70 protein-coding orphan genes were detected in each tissue. The expression level of these genes was significantly lower than other types of protein-coding genes (Additional file1: Fig. S15A and B). The median number of detected tissues for protein-coding orphan genes (one tissue) was lower than for other types of protein-coding genes (46 tissues) (Supplemental file 1: Fig. S15C). In addition, protein-coding orphan genes only transcribed protein-coding transcripts in their detected tissue(s).

Fifty percent of non-coding genes (5,559) encoded either homologous short peptides (9-43 amino acids; 5.8% of non-coding genes) or homologous ncRNAs (49% of non-coding genes) (Supplemental file 1: Fig. S14B). There were 5,546 non-coding genes (51% of non-coding genes) that encoded cattle-specific ncRNAs (Supplemental file 1: Fig. S14B). Ninety-nine percent of these genes (5,537 genes) were either known genes or genes with homology to another cattle gene(s) that has established homology to genes in other species (Supplemental file 1: Fig. S14C). The remaining 1% (nine non-coding genes) were denoted as non-coding orphan genes

(Supplemental file 1: Fig. S14C). The median number of detected tissues for non-coding orphan genes was 17 tissues, which was higher (p-value < 2.2e-16) than for homologous non-coding genes (six tissues) and protein-coding orphan genes (one tissue) (Supplemental file 1: Fig. S15C).

A total of 3,029 pseudogenes were detected. The median expression level of these genes in their detected tissues was 2.15 RPKM, which was lower than that observed for protein-coding genes (7.08 RPKM) and similar to that observed for non-coding genes (1.7 RPKM) (Supplemental file 1: Fig. S16A). Pseudogenes were detected in a median of four tissues (Supplemental file 1: Fig. S16B). The median number of detected tissues for protein-coding and non-coding genes was 44 tissues and five tissues, respectively (Supplemental file 1: Fig. S16B). In addition, a total of 1,038 pseudogene-derived lncRNAs were detected. The median expression of pseudogene-derived lncRNAs was 1.8 RPKM, similar to that observed for other lncRNAs (1.6 RPKM) (Supplemental file 1: Fig. S17A). In addition, pseudogene-derived lncRNAs were detected in a median of four different tissues, which was lower than observed for other lncRNAs (seven tissues) (Supplemental file 1: Fig. S17B).

Testis had the highest number of detected pseudogene-derived lncRNAs (427), followed by fetal brain (315) (Supplemental file 1: Fig. S8A and B). The correlation between the number of input reads and the number of pseudogene-derived lncRNAs was not significant (0.25, p-value 0.09).

Gene diversity across tissues

Tissue similarities increased dramatically from transcript level to gene level (Supplemental file 1: Fig. S4A, Fig. S5A, Fig. S18A, Fig. S19A). The median percentage of shared genes between pairs of tissues was significantly higher in protein-coding genes compared to non-coding genes (90% and 57%, respectively; p-value < 2.2e-16; Supplemental file 1: Fig. S18A, Fig. S19A). Clustering of tissues based on protein-coding genes was similar to that observed based on protein-coding transcripts (Supplemental file 1: Fig. S18B, Fig. S19B). The same result was observed in non-coding genes and transcripts. In addition, clustering of tissues based on protein-coding genes was different than that of non-coding genes (Supplemental file 1: Fig. S4B, Fig. S5B, Fig. S18B, Fig. S19B, Fig. S35F).

Tissues with both fetal and adult samples (brain, kidney, muscle, and spleen) were used to investigate gene biotype differences between these developmental stages. Similar to what was observed at transcript level, fetal tissues were significantly enriched for non-coding genes and pseudogenes and were depleted for protein-coding genes (p-value < 2.2e-16; Supplemental file 10). These results were consistent across all tissues with both adult and fetal samples (Supplemental file 10).

Gene validation

A total of 32,460 genes (92% of predicted genes) were structurally validated by independent datasets (PacBio Iso-Seq data, ONT-seq data, *de novo* assembled transcripts from RNA-seq data, or Ensembl and NCBI gene sets). In addition, a total of 31,635 genes (90% of predicted genes) were detected in multiple tissues (31,635 genes or 90%) (Fig. 7). All genes were extensively

387 supported by independent data from different technologies such as WTTS-seq, RAMPAGE,

388 histone modification (H3K4me3, H3K4me1, H3K27ac) and CTCF-DNA binding, and ATAC-seq

389 data generated from the samples.

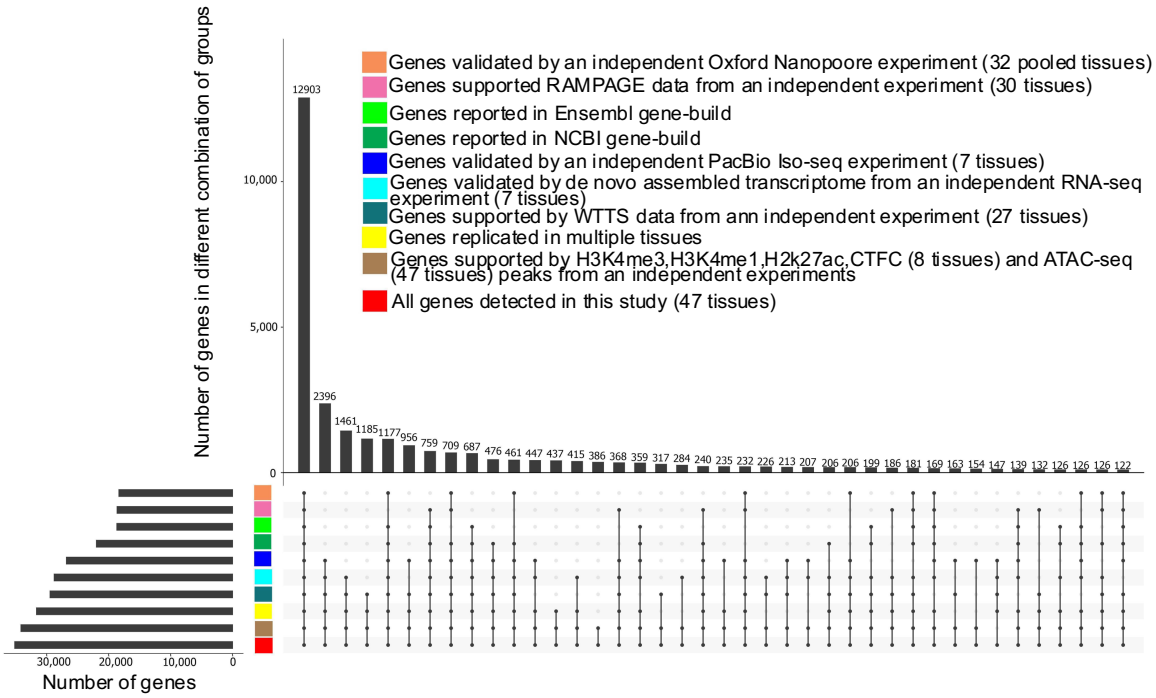

390

391 **Figure 7.** Validation of predicted genes using independent data from different technologies

392

393 **Identification and validation of known gene border extensions**

394 This new bovine gene set annotation extended (5' end extension, 3' end extension, or both)

395 more than 11,000 known Ensembl or NCBI gene borders. Extensions were longer on the 3' side,

396 but the median increase was 104 nucleotides (nt) for the 5' end (Table 5). To validate gene

397 border extensions, independent WTTS-seq (24 tissues) and RAMPAGE datasets (30 tissues)

398 were utilized. More than 80% of known gene border extensions were validated by independent
399 data (Fig. 8). The extension of known gene borders on both ends resulted in an approximate
400 nine-fold expression increase of these genes in the new bovine gene set annotation compared
401 to their matched Ensembl and NCBI genes (Table 6). This effect was smaller in known genes
402 extended only on 5' or 3' ends (Table 6).

403

Table 5. Gene border extensions in current ARS-UCD1.2 genome annotations by *de novo* assembled transcriptome from short-read RNA-seq data

Annotation	Type of gene extension	Number of genes	Median extension (nucleotides)
Ensembl	5' extension only	1,848	128
(release 2021-03)	3' extension only	5,701	422
	Both ends extended	4,874	122, 5'
			439, 3'
NCBI	5' extension only	2,214	80
(Release 106)	3' extension only	5,496	126
	Both ends extended	3,613	66, 5'
			210, 3'

404

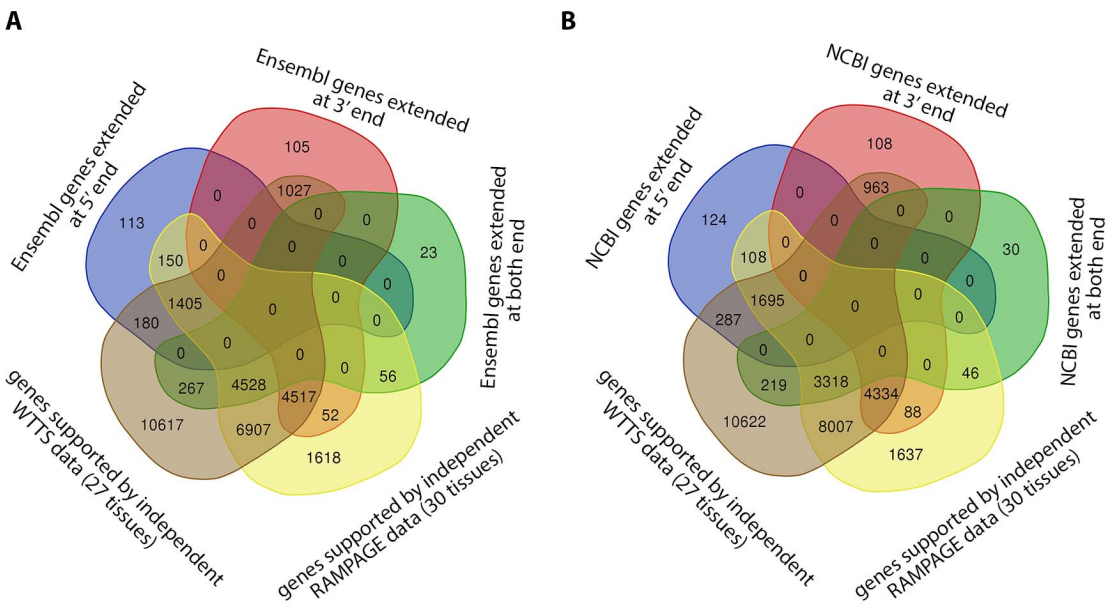

405

406 **Figure 8.** Functional enrichment analysis of non-coding genes in fetal tissues that were switched

407 to protein coding with only coding transcripts in their matched adult tissue

408

Table 6. Median number of reads mapped to the extended region of known genes[1]

Annotation	5′ end extension	3′ end extension	Both ends extension
Ensembl (release 2021-03)	92 (1.10)	220 (1.24)	1,766 (8.90)
NCBI (release 106)	72 (1.05)	95 (1.10)	2,009 (9.05)

[1]Numbers in parentheses indicate the median fold change in expression level resulting from gene extensions.

409

Alternative splicing events

Alternative splicing (AS) events (Supplemental file 1: Fig. S20A) are commonly distinguished in terms of whether RNA transcripts differ by inclusion or exclusion of an exon, in which case the exon involved is referred to as a "skipped exon" (SE) or "cassette exon", "alternative first exon", or "alternative last exon". Alternatively, spliced transcripts may also differ in the usage of a 5' splice site or 3' splice site, giving rise to alternative 5' splice site exons (A5Es) or alternative 3' splice site exons (A3Es), respectively. A sixth type of alternative splicing is referred to as "mutually exclusive exons" (MXEs), in which one of two exons is retained in RNA but not both. However, these types are not necessarily mutually exclusive; for example, an exon can have both an alternative 5' splice site and an alternative 3' splice site, or have an alternative 5' splice site or 3' splice site but be skipped in other transcripts. A seventh type of alternative splicing is "intron retention", in which two transcripts differ by the presence of an unspliced intron in one transcript that is absent in the other. An eighth type of alternative splicing is "unique splice site exons" (USEs), in which two exons overlap with no shared splice junction. A total of 102,502 bovine transcripts (80% of spliced transcripts) were involved in different types of AS events, a large increase over NCBI (73,423 transcripts) and Ensembl (37,299 transcripts) annotations (Additional file1: FigureS20B). Skipped exons were observed in a greater number of transcripts compared to other types of AS events (Supplemental file 1: Fig. S21).

A median of 60% of tissue transcripts showed at least one type of AS event (Supplemental file 1: Fig. S22A). There was no significant correlation between the number of input reads and the number of AS event transcripts across tissues (Supplemental file 1: Fig. S22B).

The median expression level of AS transcripts (111,366 transcripts or 65% of transcripts) was 1.38 RPKM, similar to that observed for other types of transcripts (1.58RPKM) (Supplemental file 1: Fig. S23A). In addition, AS transcripts were detected in a median of 10 tissues (Supplemental file 1: Fig. S23B), which was higher than for the other transcript types (median of nine tissues). AS transcripts were enriched with protein-coding transcripts (p-value < 2.2e-16). Meanwhile, transcripts that did not show AS events, i.e., unspliced transcripts and spliced transcripts from single transcript genes, were enriched for non-coding transcripts (p-value < 2.2e-16). A median of 67% of protein-coding genes showed at least one type of AS event. In contrast, this was only 3% in non-coding genes. In most cases, AS events did not change transcript biotypes (Supplemental file 1: Fig. S24). In addition, a switch from protein-coding to ncRNAs was the main biotype change resulting from AS events (Supplemental file 1: Fig. S24).

A median of four AS events were detected in alternatively spliced genes (14,260 genes or 40% of genes) (Supplemental file 1: Fig. S25). The top five percent of genes with the highest number of AS events (2,734 genes, Fig. 35A) were highly enriched for several BP GO terms related to different aspects of RNA splicing (Supplemental file 1: Fig. S26B, Supplemental file 11).

Comparison of tissues with both fetal and adult samples (brain, kidney, Latissimus Dorsi (LD) muscle, and spleen) revealed a significantly higher rate of AS events in fetal tissues (only genes expressed in both fetal and adult samples were included in this analysis) (Supplemental file 1: Fig. S27).

Tissue specificity

Nine percent of all genes (3,174) and transcripts (15,562) were only detected in a single tissue and were denoted as tissue-specific (Supplemental file 1: Fig. S28A). The majority of tissue-specific genes (75%) and transcripts (84%) were novel. Forty-nine percent of tissue-specific transcripts (11,748) were produced by known genes. The majority of tissue-specific genes (61%) and transcripts (57%) were protein-coding (Supplemental file 1: Fig. S28A and B). In addition, more than 70% of tissue-specific transcripts (11,222) were transcribed from non-tissue-specific genes. Compared to other tissues, testis and thymus had the highest number of tissue-specific genes and transcripts (Supplemental file 1: Fig. S28C, Supplemental file 12). The expression level of tissue-specific genes and transcripts was significantly lower than that of their non-tissue-specific counterparts (p-value < 2.2e-16; Supplemental file 1: Fig. S28D). A median of 71% of tissue-specific transcripts showed any type of AS event in their detected tissues (Supplemental file 1: Fig. S29). This was only 3.9% for tissue-specific genes (Supplemental file 1: Fig. S29). Testis, myoblasts, mammary gland, and thymus had the highest proportion of tissue-specific genes displaying any type of AS event (Supplemental file 1: Fig. S29).

A total of 16,806 multi-tissue detected genes (53% of all multi-tissue detected genes) and 74,487 multi-tissue detected transcripts (51% of all multi-tissue detected transcripts) showed Tissue Specificity Index (TSI) scores (Supplemental file 13) greater than 0.9 and were expressed in a tissue-specific manner. These genes and transcripts were detected in a median of six tissues and four tissues, respectively (Supplemental file 1: Fig. S30A and B). Functional enrichment analysis of the top five percent of genes with the highest TSI score (3,171 genes) resulted in the identification of “sexual reproduction” (p-value 3.06e-24) and “fertilization” (p-

472 value 1.04e-8) as their top enriched BP GO terms (Supplemental file 1: Fig. S30C-E,
473 Supplemental file 14).

474 **Tying genes to phenotypes**

475 There were 9,800 predicted genes identified as the closest gene to an existing QTL (QTL-
476 associated genes) in their detected tissues (Supplemental file 15). These genes had either QTLs
477 located inside (6,511 genes) or outside (5,306 genes) their genomic borders (either from their 5'
478 end or 3' end) with a median distance of 51.9 kilobases (KB) and a maximum distance of 2.6
479 million bases (MB) (Supplemental file 1: Fig. S31). The majority of QTL-associated genes were
480 known genes (8,130 genes or 83%). In addition, the median number of AS events in these genes
481 (eight) was significantly higher than that observed in other genes (median of seven AS events;
482 p-value 5.69e-09).

483 **Potential testis-pituitary axis**

484 Testis tissue was not clustered with any other tissues and had the highest number of tissue-
485 specific genes (1,195 genes) compared to the rest of the tissues (Supplemental file 1: Fig. S4,
486 Fig. S5, Fig. S18, and Fig. S19). Testis-specific genes were highly enriched with different traits
487 related to fertility (e.g., percentage of normal sperm and scrotal circumference), body weight
488 (e.g., body weight gain and carcass weight), and feed efficiency (e.g., residual feed intake)
489 (Supplemental file 16). The extent of testis-pituitary axis involvement in the "percentage of
490 normal sperm" was investigated using animals with both testis and pituitary samples (three
491 samples per tissue). The *SPACA5* gene was the only testis-specific gene with a (or gene
492 encoding a) signal peptide (SP) that was close to the "percentage of normal sperm" QTLs. The

493 expression of this gene in testis samples showed significant positive correlation with 70
494 pituitary genes that were closest to the “percentage of normal sperm” QTLs (Supplemental file
495 1: Fig. S32, Supplemental file 17). These pituitary genes were enriched with the “signal
496 transduction in response to DNA damage” BP GO term (Supplemental file 1: Fig. S32). In
497 addition, the expression of testis genes that encoded signal peptide that were close to the
498 “percentage of normal sperm” QTLs was significantly correlated with expression of pituitary
499 genes close to this trait (Fig. 9, Supplemental file 18). The same result was observed for the
500 pituitary-testis tissue axis (Supplemental file 1: Fig. S33, Supplemental file 19).

501

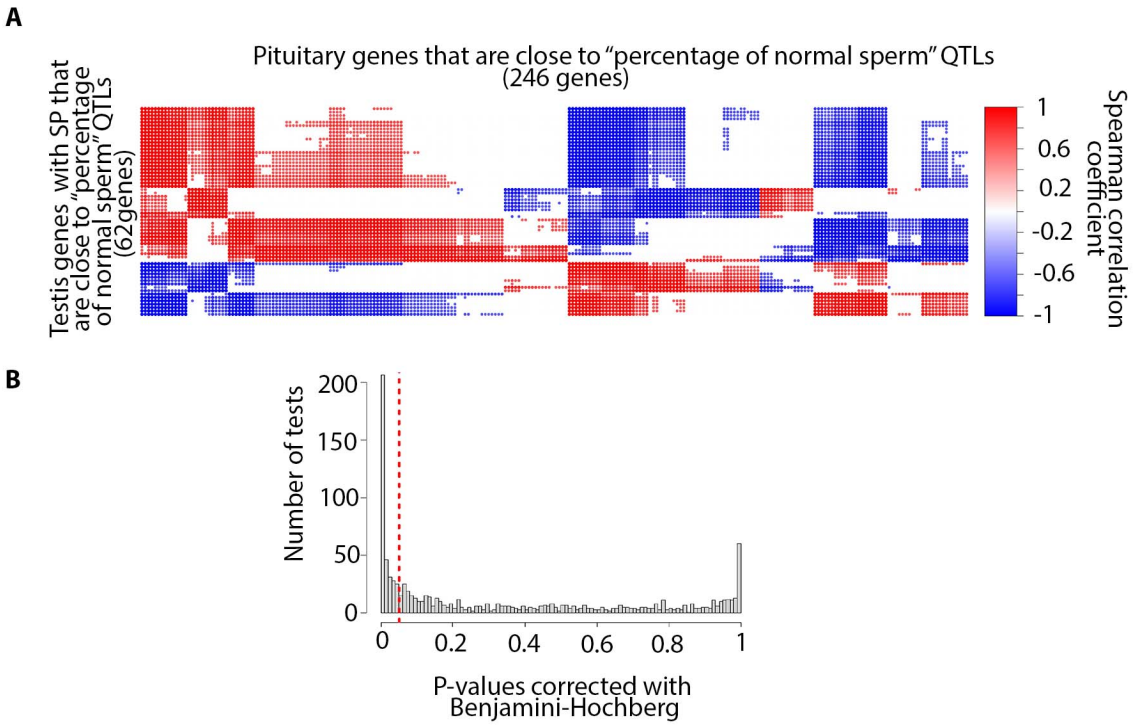

502

503 **Figure9-** (A) Correlation between testis genes with signal peptides that were close to the
504 “percentage of normal sperm” QTL and pituitary genes closest to this trait (reference

505 correlations). (B) Distribution of p-values resulting from a right-sided t-test between reference
506 correlation coefficients and correlation coefficients derived from random chance (see methods
507 for details).

508 **Trait similarity network**

509 The extent of genetic similarity between different bovine traits was investigated using their
510 associated QTLs. A total of 1,857 significantly similar trait pairs (184 different traits) were
511 identified and used to create a bovine trait similarity network
512 (https://www.animalgenome.org/host/reecylab/a; Supplemental file 20).

513 **miRNAs**

514 A total of 2,007 miRNAs (at least ten mapped reads in each tissue) comprised of 973 known and
515 1,034 novel miRNAs were detected (Supplemental file 21). In each tissue, a median of 704
516 known miRNAs and 549 novel miRNAs were detected (Fig. 10A). The median expression of
517 novel miRNAs was 0.10 Reads Per Million (RPM), which was significantly lower than that
518 observed for known miRNAs (0.41 RPM; p-value 3.25e-25; Fig. 10B). In addition, novel miRNAs
519 were detected in a median of 23 tissues, significantly lower than for known miRNAs (43 tissues;
520 p-value 1.00e-45; Fig. 10C). A median of 84.53% of miRNAs were shared between pairs of
521 tissues (Supplemental file 1: Fig. S34). Clustering of tissues based on miRNAs was similar to
522 what was observed based on non-coding genes (Supplemental file 1: Fig. S35).

523

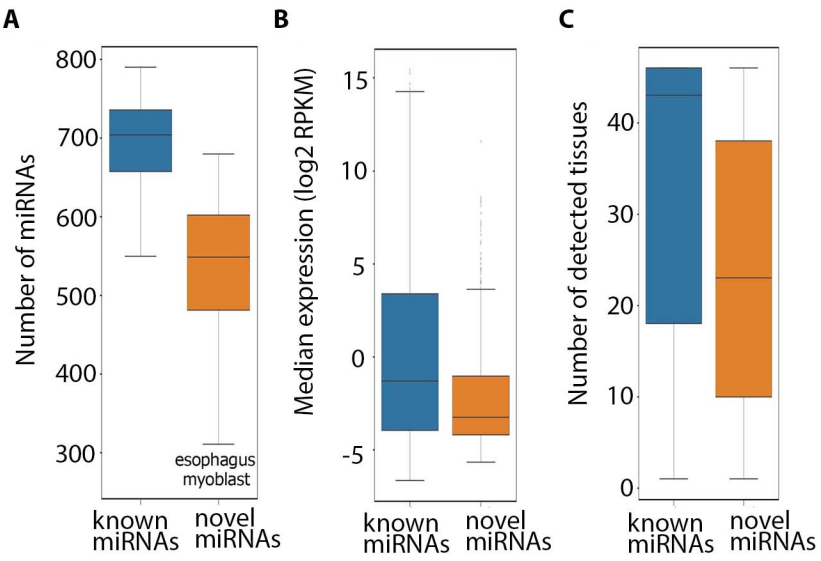

524

525 **Figure10-** (A) Distribution of the number of detected known and novel miRNAs across tissues.

526 (B) Expression of known and novel miRNAs across their detected tissues. (C) Number of

527 detected tissues for known and novel miRNAs.

528

529 A total of 113 miRNAs (5.6%) were detected in a single tissue and were denoted as tissue-

530 specific (Supplemental file 1: Fig. S36A). The proportion of tissue-specific miRNAs was higher for

531 novel miRNAs, such that 75% of the tissue-specific miRNAs (85) were novel. The number of

532 novel miRNAs was higher in pre-adipocytes compared to other tissues, followed by fetal gonad

533 and testis (Supplemental file 1: Fig. S36B). Novel miRNAs showed a significantly lower

534 expression level compared to known miRNAs (p-value 1.4e-19; Supplemental file 1: FigureS36

535 C). In addition, a total of 1,047 multi-tissue detected miRNAs (55% of all multi-tissue detected

536 miRNAs) had a TSI score greater than 0.9 and were expressed in a tissue-specific manner

(Additional file1: Fig. S36D). These miRNAs were detected in a median of 19 tissues (Supplemental file 1: Fig. S36E).

Chromatin features across 500-base pair (bp) windows surrounding upstream of miRNA precursors' start sites or downstream of miRNA precursors' terminal sites from independent cattle experiments were used to investigate the relationship between miRNAs and chromatin accessibility. More than 99% of novel miRNAs (1,027) and 94% of known miRNAs (923) were supported by at least one of the H3K4me3, H3K4me1, H3K27ac, CTCF-DNA binding, or ATAC-seq peaks (Fig. 11).

Summary of detected transcripts, genes, and miRNAs

The numbers of detected transcripts, genes, and miRNAs in different tissues are summarized in Supplemental file 1: Fig. S37. In addition, the number of known and novel genes, transcripts, and miRNAs in different tissues are summarized in Supplemental file 1: Fig. S38.

A

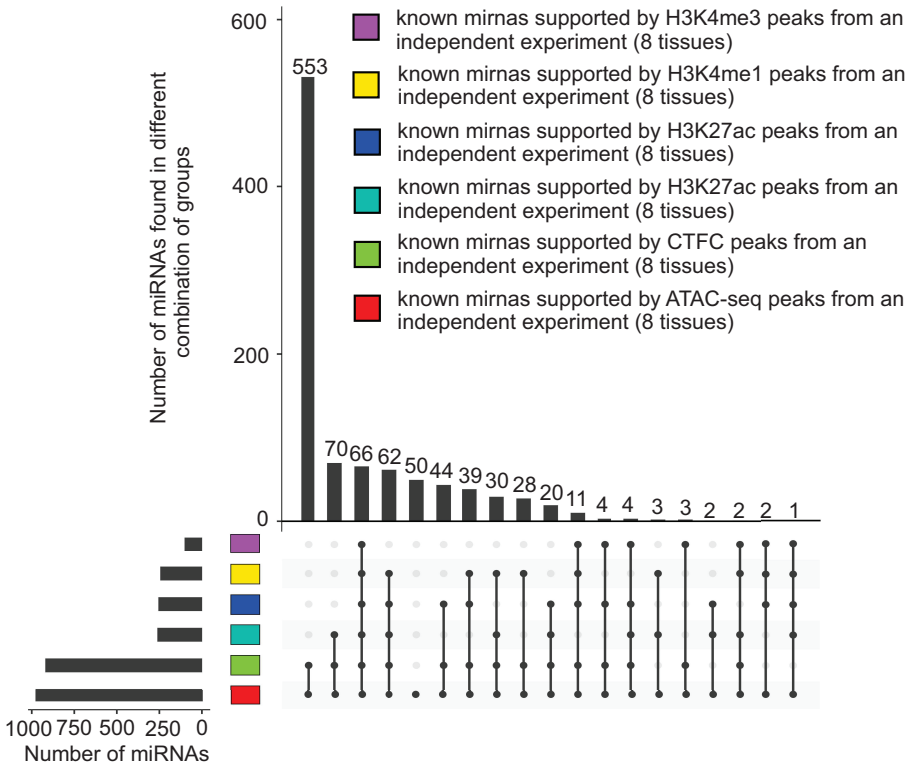

B

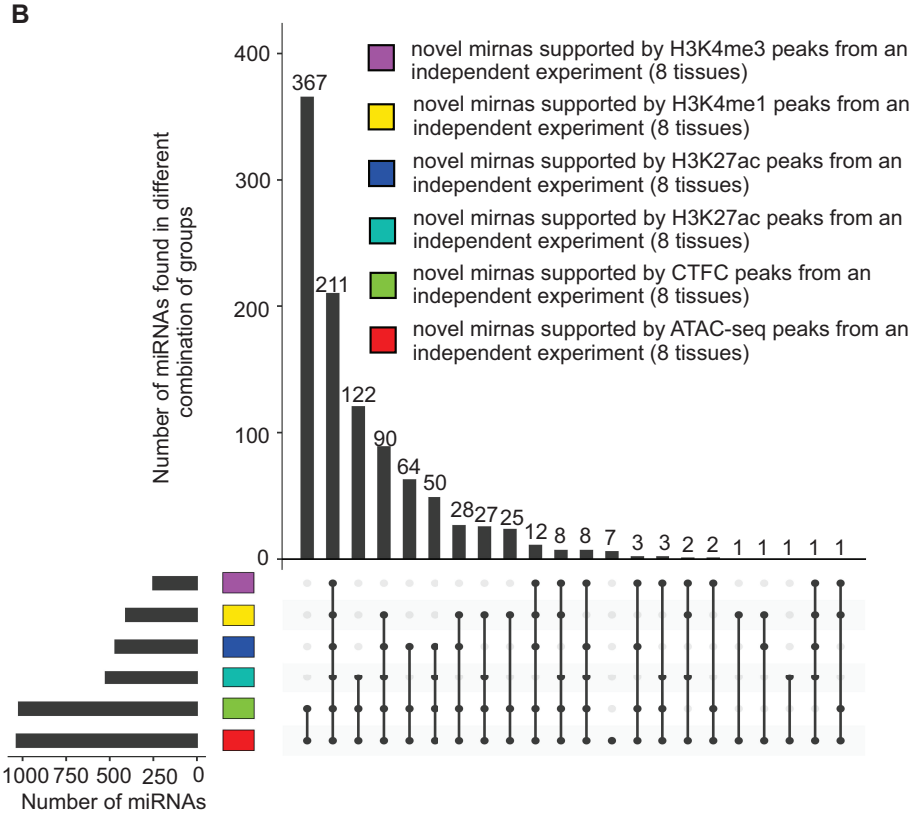

549

Figure11- Validation of detected known (A) and novel (B) miRNAs using different histone mark data

Discussion

Despite many improvements in the current bovine genome annotation ARS-UCD1.2 assembly (Ensembl release 2021-03 and NCBI release 106) compared to the previous genome assembly (UMD3.1), these annotations are still far from complete (Goszczynski et al. 2021; Halstead et al. 2021). In this study, using RNA-seq and miRNA-seq data from 47 different bovine tissues/cell types, 12,698 novel genes and 1,034 novel miRNAs were identified that have not been reported in current bovine genome annotations (Ensembl release 2021-03, NCBI release 106 and miRbase (Kozomara et al. 2019)). In addition, we identified protein-coding transcripts with a median ORF length of 270 nt for 822 known bovine genes that have been annotated as non-coding in current bovine genome annotations (Supplemental file 1: Fig. S14C). The high frequency of validation of these novel genes and novel miRNAs using multiple independent datasets from different technologies verifies the improvement in terms of the number of genes and miRNAs using our methods.

Five prime and 3‘untranslated region length plays a critical role in regulation of mRNA stability, translation, and localization (Jereb et al. 2018). However, only a single 5’ UTR and 3’ UTR per gene is annotated in current bovine genome annotations (Ensembl release 2021-03 and NCBI release 106), and variations in UTR length are not available. In this study, 7,909 genes (22% of predicted genes) with multiple UTRs were identified. Genes with multiple 5’ UTRs are common, primarily due to the presence of multiple promoters (Araujo et al. 2012) or alternative splicing

571 mechanisms within 5' UTRs (Araujo et al. 2012). Fifty-four percent of human genes have
572 multiple transcription start sites (Araujo et al. 2012). In addition, the length of 3' UTRs often
573 varies within a given gene, due to the use of different poly-adenylation (polyA) sites (Jereb et al.
574 2018; Gerber et al. 2021).

575 In this study, around 50% of detected protein-coding genes in each tissue transcribed both
576 coding and non-coding transcript isoforms. Several studies have shown evidence of the
577 existence of bifunctional genes with coding and non-coding potential using high-throughput
578 RNA sequencing (RNA-seq) and ribosome footprinting followed by sequencing (Ribo-seq)
579 (Andrews and Rothnagel 2014; Kumari and Sampath 2015; Nam et al. 2016). More than 20% of
580 human protein-coding genes have been reported to transcribe non-coding isoforms, often
581 generated by alternative splicing (Gonzàlez-Porta et al. 2013) and recurrently expressed across
582 tissues and cell lines (Nam et al. 2016). A considerable number of non-coding isoform variants
583 of protein-coding genes appear to be sufficiently stable to have functional roles in cells (Mayba
584 et al. 2014). It has been shown that the proportion of non-coding isoforms from protein-coding
585 genes dramatically increases during myogenic differentiation of primary human satellite cells
586 and decreases in myotonic dystrophy muscles (Hubé et al. 2011). In this study, 106 non-coding
587 genes were identified in fetal tissues that switched to protein-coding genes in their matched
588 adult tissues. Taken together this supports the notion that protein-coding/non-coding
589 transcript switching plays an important role in tissue development in cattle as well.

590 Nonsense-mediated RNA decay is an evolutionarily conserved process involved in RNA quality
591 control and gene regulatory mechanisms (Kurosaki et al. 2019). For instance, the RNA-binding
592 protein polypyrimidine tract binding protein 1 (*PTBP1*) can promote the transcription of NMD

593 transcripts via alternative splicing, which negatively regulates its own expression (Wollerton et
594 al. 2004). In this study, NMD transcripts comprised 19% of bovine transcripts that were
595 transcribed from 30% of bovine genes (10,498). In humans, NMD-mediated degradation can
596 affect up to 25% of transcripts (Nickless et al. 2017) and 53% of genes (Supek et al. 2021). As
597 expected, in this study, the majority of genes that transcribed NMD transcripts were protein
598 coding (83% or 8,687 genes), while a considerable portion (17%) were pseudogenes. Many
599 pseudogenes are known to give rise to NMD transcripts (Mitrovich and Anderson 2005;
600 Colombo et al. 2017). Bioinformatic study of the human transcriptome revealed that 78% of
601 NMD transcript–producing genes were protein coding, followed by pseudogenes (nine percent),
602 long intergenic noncoding RNAs (six percent), and antisense transcripts (four percent) (Colombo
603 et al. 2017).

604 Despite the important regulatory function of lncRNAs and miRNAs, very low numbers of these
605 elements have been annotated in the current bovine genome annotations (Table 7). In this
606 study, a total of 10,789 lncRNA genes and 2,007 miRNA genes were detected in the bovine
607 transcriptome, which is similar to what has been reported for the human transcriptome (Table
608 7). While, a total of 3,770 human miRNAs and 1,203 cattle miRNAs have been reported in
609 miRbase (Kozomara et al. 2019). Small non-coding RNAs detected from RNA-seq data did not
610 overlap with known or novel miRNA precursors or known sncRNAs reported in Ensembl or NCBI
611 gene builds.

612

613

614

Table 7. Comparison of different gene builds based on gene biotypes

Species	Gene build	Protein-coding genes	lncRNA genes	miRNA genes	Other types of small non-coding genes[1]	Pseudo-genes
Bovine (ARS-UCD1.2)	Ensembl (Release 2021-03)	21,880	1,480	951	2,209	492
	NCBI (Release 106)	21,039	5,179	797	3,249	4,569
	Cattle FAANG[2]	21,193 (18,096)	10,789 (2,847)	2,007 (973)	139 (0)	3,029 (1,509)
Human (GRCh38.104)	Ensembl (release 2021-03)	20,442	16,876	1,877	2,930	15,266

[1]Small nucleolar RNAs, small nuclear RNAs, small Cajal body specific RNAs, small conditional RNAs, and tRNAs

[2]Numbers in parentheses indicate the number of novel RNAs in each biotype.

615

In this study, 1,038 pseudogene-derived lncRNAs were identified that were recurrently expressed across tissues and cell types. Ever-increasing evidence from different studies suggests pseudogene-expressed RNAs are key components of lncRNAs (Milligan and Lipovich 2014; Stewart et al. 2019; Lou et al. 2020). lncRNAs expressed from pseudogenes have been shown to regulate genes with which they have sequence homology (Milligan and Lipovich 2014; Stewart et al. 2019) or to coordinate development and disease in metazoan systems (Milligan and Lipovich 2014).

Correct annotation of gene borders has an important role in defining promoter and regulatory regions. Our novel transcriptome analysis extended (5'-end extension, 3'-end extension, or both) more than 11,000 known Ensembl or NCBI gene borders. Extensions were longer on the 3' side, which was relatively similar to that we observed in the pig transcriptome using PacBio Iso-Seq data (Beiki et al. 2019).

A growing body of evidence indicates that a considerably large portion of lncRNAs encode microproteins that are less conserved than canonical Open Reading Frames (ORFs) (Anderson et al. 2015; Mackowiak et al. 2015; Olexiouk et al. 2016; Li and Liu 2019; Wei and Guo 2020). In this study, a vast majority (98%) of predicted lncRNAs had short ORFs (<44 amino acids) that were less conserved than canonical ORFs (Table 2).

Alternative splicing is the key mechanism to increase the diversity of the mRNA expressed from the genome and is therefore essential for response to diverse environments. In this study, skipped exons and retained introns were the most prevalent AS events identified in the bovine transcriptome, similar to what has been observed in other vertebrates and invertebrates

637 (Sammeth et al. 2008). A higher rate of AS events was observed in fetal tissues compared to
638 their adult tissue counterparts. The same result has been observed in a recently published
639 study in humans (Mazin et al. 2021).

640 We hypothesized that the integration of the gene/transcript data with previously published
641 QTL/gene association data would allow for the identification of potential molecular
642 mechanisms responsible for a) tissue-tissue communication as well as b) genetic correlations
643 between traits. To test the first hypothesis, we developed a novel approach to study the
644 involvement of tissue-tissue interconnection in different traits based on the integration of the
645 transcriptome with publicly available QTL data. In particular, the interconnection between
646 testis and pituitary tissues with respect to the “percentage of normal sperm” trait was
647 investigated in more detail. This resulted in the identification of the regulation of ubiquitin-
648 dependent protein catabolic process, the regulation of Nuclear factor-κB (NF-κB) transcription
649 factor activity, and Rab protein signal transduction as key components of this tissue-tissue
650 interaction (Supplemental file 18 and 19). Interestingly, genes that were closest to “percentage
651 of normal sperm” QTLs, and also encoded signal peptides in both testis and pituitary tissues,
652 were highly enriched for the BP GO term “regulation of ubiquitin-dependent protein catabolic
653 process” (Supplemental file 18 and 19). The expression of these genes in testis tissue was
654 significantly correlated with expression levels of pituitary genes closest to “percentage of
655 normal sperm” QTLs that were highly enriched for the “positive regulation of NF-kappaB
656 transcription factor activity” BP GO term (Supplemental file 1: Fig. S32 and Supplemental file
657 18). Activation of NF-κB requires ubiquitination, and this modification is highly conserved across
658 different species (Chen and Chen 2013). NF-κB induces secretion of adrenocorticotropic

659 hormone from the pituitary (Karalis et al. 2004), which directly stimulates testosterone
660 production by the testis (O'Shaughnessy et al. 2003). In addition, ubiquitinated proteins in testis
661 cells are required for the progression of mature spermatozoa (Richburg et al. 2014). The
662 expression levels of pituitary genes closest to “percentage of normal sperm” QTLs that also
663 encoded signal peptides were significantly correlated with expression levels of testis genes
664 closest to “percentage of normal sperm” QTLs (Supplemental file 1: Fig. S33). These testis genes
665 were highly enriched for the “Rab protein signal transduction” BP GO term (Supplemental file
666 19). Rab proteins have been reported to be involved in male germ cell development (Kumar et
667 al. 2016). Thus, it appears that integration of gene data with QTL/association data can be used
668 to identify putative molecular pathways underlying tissue-tissue communication mechanisms.

669 To test the second hypothesis, we also developed a novel approach to study trait similarities
670 based on the integration of the transcriptome with publicly available QTL data. Using this
671 approach, we could identify significant similarity between 184 different bovine traits. For
672 example, clinical mastitis showed significant similarity with 23 different cattle traits that were
673 greatly supported by published studies, such as milk yield (Rajala-Schultz et al. 1999), milk
674 composition traits (Martí De Olives et al. 2013), somatic cell score (Halasa and Kirkeby 2020),
675 foot traits (Remnant et al. 2019), udder traits (Miles et al. 2019), daughter pregnancy rate (Lima
676 et al. 2020), length of productive life (Hertl et al. 2018) and net merit (Kaniyamattam et al.
677 2020). Similar results were observed for residual feed intake, which showed significant
678 similarity with 14 different traits such as average daily feed intake (Green et al. 2013), average
679 daily gain (Elolimy et al. 2018), carcass weight (Weber et al. 2013), feed conversion ratio (Yi et

al. 2018), metabolic body weight (Liu and VandeHaar 2020), subcutaneous fat (Clare et al. 2018), and dry matter intake (Houlahan et al. 2021).

Taken together, these results identify a list of candidate genes that might harbor genetic variation responsible for the genetic mechanisms underlying genetic correlations (Supplemental file 18 and 1. If this is the case, in the future, these novel methods should be able to predict the impact of a given set of genetic variants that are associated with a trait of interest on other traits that were not measured in a given study. This might then lead to the optimization of variants used (or not used) in genomic selection to minimize any non-beneficial effect of selection on selected traits.

Conclusions

In-depth analysis of multi-omics data from 47 different bovine tissues/cell types provided evidence to improve the annotation of thousands of protein-coding, lncRNA, and miRNA genes. These validated results increase the complexity of the bovine transcriptome (number of transcripts per gene, number of UTRs per gene, lncRNA transcripts, AS events, and miRNAs), comparable to that reported for the highly annotated human genome. We provided direct evidence that the predicted novel transcripts extend existing known gene models, by verifying such extensions using independent WTTS-seq and RAMPAGE data. We utilized a novel approach to integrate the transcriptome with publicly available QTL data and showed its application in a study of tissue axis involvement in different traits and genetic similarity between different traits. This approach is particularly important in the selection of indicator

traits for breeding purposes, study of artificial selection side effects in livestock species, and functional annotation of poorly annotated livestock genomes.

Methods

Tissue and cell collection, total RNA extraction and construction of RNA-seq, miRNA-seq, WTTS-seq, ATAC-seq, and ChIP-seq libraries

Cell sample collections. Skeletal muscle and subcutaneous fat samples were collected from Angus-crossbred steers slaughtered at the Virginia Tech Meat Center. Satellite cells were isolated from skeletal muscle by pronase digestion as described previously (Leng et al. 2019). The isolated satellite cells were activated to proliferate as myoblasts by culturing in growth medium composed of Dulbecco's Modified Eagle Medium (DMEM), 10% fetal bovine serum (FBS), and 1% antibiotics-antimycotics. To induce myoblasts to differentiate into myocytes, myoblasts cultured in growth medium were switched to differentiation medium composed of DMEM and 2% horse serum for 2 days. Preadipocytes from subcutaneous fat were isolated by collagenase digestion as previously described (Hausman et al. 2008). To induce preadipocytes to differentiate into adipocytes, preadipocytes were initially cultured in growth medium (DMEM/F12, 10% FBS, 1% antibiotics-antimycotics) to reach confluency, then in induction medium (DMEM/F12, 10% FBS, 1% antibiotics-antimycotics, 10 µg/mL insulin, 1 µM dexamethasone, 0.5 mM isobutyl methylxanthine, and 200 µM indomethacin) for 2 days, and lastly in maintenance medium (DMEM/F12, 10% FBS, 1% antibiotics-antimycotics, 1 µg/mL insulin) for 10 days.

720 **Adult tissue collections.** Procedures for tissue collection followed the Animal Care and Use
721 protocol (#18464) approved by the Institutional Animal Care and Use Committee (IACUC),
722 University of California, Davis (UCD). Four cattle (2 males and 2 females) were slaughtered at
723 UCD using captive bolt under USDA inspection at 14 months old and were intact male and
724 female Line 1 Herefords that had the same sire, provided by Fort Keogh Livestock and Range
725 Research Lab (Tixier-Boichard et al. 2021). Tissue samples were flash frozen in liquid nitrogen
726 then stored at –80 °C until further assay processing.

727 **Fetal tissue collections.** Fetal sample collection and tissue collection were approved by the
728 Institutional Animal Care and Use Committee (IACUC), University of Idaho (2017-67). Four
729 pregnant females at day 78 of gestation Line 1 Herefords were slaughtered at UI meats lab
730 using captive bolt under USDA inspection. Animals were provided by Fort Keogh Livestock and
731 Range Research Lab (Tixier-Boichard et al. 2021). Tissue samples were flash frozen in liquid
732 nitrogen then stored at –80 °C until further assay processing.

733 **RNA-seq library construction.** Tissue samples (Supplemental file 22) were collected from
734 storage at -80 °C and ground to a powder using a mortar and pestle and liquid nitrogen. The
735 tissue was next homogenized in QIAzol Lysis Reagent (Qiagen Catalog No. 79306) using a
736 QIAshredder spin column (Qiagen Catalog No. 79656). After centrifugation, the lysate was
737 mixed with chloroform, shaken vigorously for 15 sec, incubated for 2 – 3 min at room
738 temperature, and centrifuged for 15 min at 12,000 x g at 4°C. The upper, aqueous phase was
739 transferred to a new collection tube and 1.5 vol of 100% ethanol was added and mixed
740 thoroughly by pipetting up and down several times. Total RNA was then isolated from the

741 sample using the RNeasy Mini Kit (Qiagen Catalog No. 74106) according to the manufacturer's
742 instructions. Contaminating DNA was removed by treating total RNA with DNase (AM1906,
743 Ambion). Total RNA quantity was measured with the Quant-It RiboGreen RNA Assay Kit (Life
744 Technologies Corp., Carlsbad, CA) and quality assessed by fragment analysis (Advance Analytical
745 Technologies, Inc., Ankeny IA).

746 **Mammary gland tissue collection and RNA-seq library construction.** The 16 animals used in
747 this study were Holstein-Friesian heifers from a single herd managed at the AgResearch
748 Research Station in Ruakura, NZ. All experimental protocols were approved by the AgResearch,
749 NZ, ethics committee, and carried out according to their guidelines. Samples were collected
750 from the same animals at 5 time points: virgin state before pregnancy between 13 and 15
751 months of age (virgin), mid-pregnant at day 100 of pregnancy, late pregnant ~2 weeks pre-
752 calving, early lactation ~2 weeks post-calving, and at peak lactation, 34-38 days post-calving.
753 Tissue samples were obtained by mammary biopsy using the Farr method (Farr et al. 1996).
754 Lactating cows were milked before biopsy and sampled within 5 hours of milking. Biopsy sites
755 were clipped and given aseptic skin preparation (povidone iodine base scrub and iodine
756 tincture) and subcutaneous local anesthetic (4 ml per biopsy site). Core biopsies were taken
757 using a powered sampling cannula (4.5 mm internal diameter) inserted into a 2 cm incision. The
758 resulting samples of mammary gland parenchyma measured 70 mm in length, with a 4 mm
759 diameter. Small slices from each sample were preserved for histology before mammary
760 epithelial organoids were separated from surrounding adipose and connective tissue to allow
761 for secretory-specific signals in the RNA-seq analysis. In preparation for isolating organoids,
762 tissue samples were digested in a freshly prepared collagenase solution containing 0.2%

763 collagenase A (Roche), 0.05% trypsin (1:250 powder, 100U/ml Gibco), hyaluronidase (Sigma),
764 5% fetal calf serum (Hyclone), Pen/Strep/Fungizone solution (Hyclone) or 5 µg/ml Gentamycin
765 (Sigma) in DMEM/F12 (Gibco) with 10 ng/ml insulin. Samples were minced to a fine slurry and
766 incubated in this freshly prepared collagenase solution (10 ml solution/g tissue) for 3.5 hours at
767 37°C in a 50 ml conical tube with slow shaking (120 rpm). Digested tissue was centrifuged at
768 453 x g for 10 min at 4°C, after which the supernatant and fat layers were discarded, and the
769 pellet was gently resuspended in 5 ml DMEM/F12 without serum. A further 5 ml DMEM/F12
770 without serum was added, and the sample was centrifuged at 453 x g for 10 min at 4°C. The
771 media was discarded, and the pellet was gently resuspended in 10 ml DMEM/F12 and
772 centrifuged for another 10 min at 453 x g and 4°C. The media was discarded, and pellet
773 resuspended in 10 ml DMEM/F12 for a third time, and the sample centrifuged in a series of
774 brief spins achieved by allowing the centrifuge to reach 453 x g for two seconds before applying
775 the brake. These brief pulse spins were repeated at least 4 times, or until examining the sample
776 under a microscope revealed primarily epithelial organoid clusters and very few single cells. At
777 this point, the organoid pellet was resuspended in 1 ml TRIzol and stored at -80°C until RNA
778 isolation. High-quality total RNA (RIN > 7) was extracted from frozen mammary epithelial
779 organoid pellets using NucleoSpin® miRNA isolation kit (MACHEREY-NAGEL) according to the
780 manufacturer's protocol, isolating large and small (<200 nt) fractions separately. The "large"
781 RNA fraction was used to prepare strand-specific poly-A+ RNA-seq libraries for sequencing. The
782 "small" RNA fraction was used to make miRNA-seq libraries using NEXTflex™ Small RNA-Seq Kit
783 v3.

784 **miRNA-seq library construction.** Tissue samples (Supplemental file 22) were collected similarly
785 to the method described in the previous section. QIAseq miRNA Library Kit (Qiagen, cat no.
786 331505) and QIAseq miRNA NGS 96 Index IL Kit (Qiagen, cat no. 331565) were used to isolate
787 miRNAs from all tissues except mammary gland. miRNAs from mammary gland were isolated
788 using NEXTflex^{TM} Small RNA-Seq Kit v3 (Illumina) according to the manufacturer's instructions.
789 The isolated miRNA was subjected to 3' ligation to ligate a pre-adenylated DNA adaptor to the
790 3' ends of all miRNAs. An RNA adaptor was then ligated to the 5' end of the mature miRNA to
791 complete 5' ligation. cDNA synthesis was completed using a reverse transcriptase (RT) primer
792 containing integrated unique molecular identifiers (UMI). The RT primer bound to the 3'
793 adaptor region and facilitated conversion of the 3'/5' ligated miRNAs into cDNA while a UMI
794 was assigned to every miRNA molecule. After reverse transcription, a clean-up of the cDNA was
795 performed using a streamlined magnetic bead-based method. Library amplification was
796 accomplished by a universal forward primer from a plate being paired with 1 of 96 dried
797 reverse primers in the same plate (Qiagen, cat no. 331565) to assign each sample a unique
798 custom index. Following library amplification, a clean-up of the miRNA library was performed
799 using a streamlined magnetic bead-based method. Libraries were then evaluated for quantity
800 and quality measures before being normalized and pooled for llumina sequencing (1×50bp).

801 **WTTS-seq library construction.** Construction of the WTTS-seq libraries from tissue samples
802 (Supplemental file 22) involved fragmentation, polyA+ RNA enrichment, first-strand cDNA
803 synthesis by reverse transcription and second-strand cDNA synthesis by PCR as described
804 previously (Zhou et al. 2016). The starting material was 2.5 µg of total RNA per library, which
805 was fragmented with 1 µl of 10X RNA fragmentation buffer (Ambion, AM8740), followed by

806 enrichment of polyA+ RNA using Dynabeads (Ambion 61002). The polyA+ RNA molecules were
807 then used for the first-strand cDNA synthesis with both 5' adaptor (switching primer, 100 µM)
808 and 3' adaptor (containing oligo (dT10), 100 µM) catalyzed by the SuperScript III reverse
809 transcriptase (200 U/µl) (Invitrogen, 18080). The first-strand cDNA molecules were chemically
810 enriched with RNases I and H and used to synthesize the second-strand cDNA using PCR. Base
811 PCR conditions were as follow: initial denaturation at 98 °C for 30 s, PCR cycles of 98 °C for 10 s,
812 50°C for 30 s, and 72°C for 30 s, and final extension at 72°C for 10 min. The size-selected cDNA
813 (200 – 500 bp) was purified with SPRI beads (Agencourt AMPure XP beads, Beckman Coulter,
814 Brea, CA) and sequenced using an Ion PGM™ Sequencer at Washington State University.

815 **ChIP-seq library construction.** ChIP-seq experiments (H3K4me3, H3K4me1, H3K27ac and
816 H3K27me3) were performed on flash-frozen tissue samples (Supplemental file 22) using the
817 iDeal ChIP-seq kit (Diagenode Cat. #C01010059, Denville, NJ). Briefly, 20–30 mg powdered
818 tissue was cross-linked with 1% formaldehyde for 8 min and quenched with 100 µl of glycine for
819 10 min. Nuclei were obtained by centrifugation at 2000 × g for 5 min and resuspended in 600 µl
820 of iS1 buffer for incubation on ice for 30 min. Chromatin was sheared using the Bioruptor Pico
821 between 10 and 15 cycles depending on the tissues. For immunoprecipitation experiments, ~1–
822 1.5 µg of sheared chromatin was used as input with 1 µg (histone modifications) or 1.5 µg
823 (CTCF) of antibody following the protocol from the kit. The following antibodies used were from
824 Diagenode: H3K4me3 (comes with Diagenode iDeal Histone kit), H3K27me3 (#C15410069),
825 H3K27ac (#C15410174), H3K4me1 (#C15410037), and CTCF (#15410210). An input (no
826 antibody) was performed for each sample. Libraries were constructed using the NEBNext Ultra

827 DNA library prep kit (New England Biolabs #E7645L, Ipswich, MA). Libraries were sequenced on
828 the Illumina HiSeq 4000 platform, generating 50 bp single-end reads.

829 **ATAC-seq library construction.** Frozen tissue samples (Supplemental file 22) were pulverized
830 under liquid nitrogen using mortar and pestle. Permeabilized nuclei were obtained by
831 resuspending pulverized tissue (5-15 mg) in 250 µL Nuclear Permeabilization Buffer (0.2%
832 IGEPAL-CA630 [I8896, Sigma], 1 mM DTT [D9779, Sigma], Protease inhibitor [05056489001,
833 Roche], and 5% BSA [A7906, Sigma] in PBS [10010-23, Thermo Fisher Scientific]), and incubating
834 for 10 min on a rotator at 4°C. Nuclei were then pelleted by centrifugation for 5 min at 500 x g
835 at 4°C. The pellet was resuspended in 25 µL ice-cold Tagmentation Buffer (33 mM Tris-acetate
836 [pH = 7.8; BP-152, Thermo Fisher Scientific], 66 mM K-acetate [P5708, Sigma], 11 mM Mg-
837 acetate [M2545, Sigma], 16% DMF [DX1730, EMD Millipore] in molecular biology grade water
838 [46000-CM, Corning]). An aliquot was then taken and counted by hemocytometer to determine
839 nuclei concentration. Approximately 50,000 nuclei were resuspended in 20 µL ice-cold
840 Tagmentation Buffer and incubated with 1 µL Tagmentation enzyme (FC-121-1030, Illumina) at
841 37 °C for 30 min with shaking at 500 rpm. The tagmentated DNA was purified using MinElute
842 PCR purification kit (28004, Qiagen). The libraries were amplified using NEBNext High-Fidelity
843 2X PCR Master Mix (M0541, NEB) with primer extension at 72°C for 5 min, denaturation at 98°C
844 for 30 s, followed by 8 cycles of denaturation at 98°C for 10 s, annealing at 63°C for 30 s and
845 extension at 72°C for 60 s. Amplified libraries were then purified using MinElute PCR
846 purification kit (28004, Qiagen), and two size selection steps were performed using SPRIselect
847 bead (B23317, Beckman Coulter) at 0.55X and 1.5X bead-to-sample volume ratios, respectively.

ATAC-seq libraries were sequenced on an Illumina Nextseq 500 platform using Nextra V2 sequencing chemistry to generate 2 × 75 paired-end reads.

Sequencing the transcriptomes of seven bovine tissues by using the PacBio Iso-Seq and Illumina RNA-Seq technologies

Frozen tissue samples (Supplemental file 22) were pulverized by grinding with disposable mortar and pestle in liquid nitrogen. RNA was extracted using TRIzol reagent as directed by the manufacturer (Invitrogen) with integrity examined using a BioAnalyzer (Agilent). Only samples with RIN values >8 were used for cDNA synthesis. Libraries for RNA-seq short-read sequencing were prepared using the TruSeq RNA Kit following the "TruSeq RNA Sample Preparation v2 Guide" as recommended by the manufacturer (Illumina). RNA-seq libraries were sequenced on a NextSeq500 instrument. IsoSeq libraries for long-read sequencing were prepared using the SMRTbell Template Prep Kit 1.0. First strand cDNA synthesis was performed with approximately 1 µg of extracted RNA from each tissue using the Clontech SMARTer PCR cDNA Synthesis Kit (Clontech) as directed by the manufacturer. cDNA was then converted to SMRTbell template library following the "Iso-Seq using Clontech cDNA Synthesis and BluePippin Size Selection" protocol as directed by the manufacturer (Pacific Biosciences). Three size fraction pools for each tissue were prepared using the BluePippin instrument (Sage Science), representing insert sizes of 1-2 kb, 2-3 kb, and 3-6 kb. The two smaller fractions were sequenced in three to five SMRT cells on an RSII instrument (Pacific Biosciences), and the largest fraction sequenced in five or six cells, using P6/C4 chemistry. The sequences were processed into HQ isoforms using SMRT Analysis v6.0 for each tissue independently but with all size fractions within tissue included in the analysis.

RNA-seq data analysis and transcriptome assembly

Single-end Illumina RNA-Seq reads (75 bp) from each tissue sample were trimmed to remove the adaptor sequences and low-quality bases using Trim Galore (version 0.6.4) (Krueger 2019) with --quality 20 and --length 20 option settings. The resulting reads were aligned against ARS-UCD1.2 bovine genome using STAR (version 020201) (Dobin et al. 2013) with a cut-off of 95% identity and 90% coverage. FeatureCounts (version 2.0.2) (Liao et al. 2014) was used to quantify genes reported in the NCBI gene build (version 1.21) with -Q 255 -s 2 --ignoreDup --minOverlap 5 option settings. The resulting gene counts were adjusted for library size and converted to Counts Per Million (CPM) values using SVA R package (version 3.30.0) (Leek et al. 2021). In each tissue, sample similarities were checked using hierarchical clustering and regression analysis of gene expression values (log2 based CPM), and outlier samples were detected and removed from downstream analysis. Samples from each tissue were combined to get the most comprehensive set of data in each tissue. To reduce the processing time due to huge sequencing depth, the trimmed reads were in silico normalized using insilico_read_normalization.pl from Trinity package (version 2.6.6) (Grabherr et al. 2011) with --JM 350G and --max_cov 50 option settings. Normalized RNA-seq reads were aligned against ARS-UCD1.2 bovine genome using STAR (version 020201) (Dobin et al. 2013) with a cut-off of 95% identity and 90% coverage. The normalized reads were assembled using *de novo* Trinity software (version 2.6.6) (Grabherr et al. 2011) combined with massively parallelized computing using HPCgridRunner (v1.0.1) (Hass 2015) and GNU parallel software (Tange 2018). The resulting transcript reads were collapsed and grouped into putative gene models (clustering transcripts that had at least a one-nucleotide overlap) by the pbtranscript-ToFU from SMRT

892 Analysis software (v2.3.0) (PacificBiosciences 2018) with min-identity = 95%, min-
893 coverage = 90% and max_fuzzy_junction = 15 bp, whereas the 5'-end and 3'-end difference
894 were not considered when collapsing the reads. Base coverage of the resulting transcripts was
895 calculated using mosdepth (version 0.2.5) (Pedersen and Quinlan 2018). Predicted transcripts
896 were required to have a minimum of three times base coverage in their detected tissues. The
897 predicted acceptor and donor splice sites were required to be canonical and supported by
898 Illumina-seq reads that spanned the splice junction with 5-nt overhang. Spliced transcripts with
899 the exact same splice junctions as their reference transcripts but that contained retained
900 introns were removed from analysis, as they were likely pre-RNA sequences. Unspliced
901 transcripts with a stretch of at least 20 A's (allowing one mismatch) in a genomic window
902 covering 30 bp downstream of their putative terminal site were removed from analysis, as they
903 were likely gDNA contaminations. To decrease the false positive rate, unspliced transcripts that
904 were only detected in a single tissue were removed from downstream analysis. The resulting
905 transcripts from each tissue were re-grouped into gene models using an in-house Python script.
906 The collapsed transcripts from the different tissues were then merged using an in-house Python
907 script to create the RNA-seq based bovine transcriptome.

908 The resulting transcripts and genes were quantified using align_and_estimate_abundance.pl
909 from the Trinity package (version 2.6.6) (Grabherr et al. 2011) with --aln_method bowtie --
910 est_method RSEM --SS_lib_type RF option settings.

911 "Isoform" and "transcript" terms are used interchangeably throughout the manuscript.

912 **PacBio Iso-Seq data analysis**

913 PacBio Iso-Seq data has been processed as described for the pig transcriptome (Beiki et al.
914 2019) with the following exceptions. Errors in the full-length, non-chimeric (FLNC) cDNA reads
915 were corrected with the preprocessed RNA-Seq reads from the same tissue samples using the
916 combination of proovread (v2.12) (Hackl et al. 2014) and FMLRC (v1.0.0) (Wang et al. 2018)
917 software packages. Error rates were computed as the sum of the numbers of bases of
918 insertions, deletions, and substitutions in the aligned FLCN error-corrected reads divided by the
919 length of aligned regions for each read (Table 8).

920 The RNA-seq-based transcriptome was assembled as described in the previous section.

921

Table 8. Summary of error-corrected, full-length non-chimeric (FLNC) Iso-Seq reads and their matched RNA-seq reads

Tissue	Error-corrected FLNC Iso-Seq reads[1]	Median error rate in error-corrected FLNC Iso-Seq reads	Normalized RNA-seq reads used for error correction[2]
Thalamus	664,900 (90%)	0.21%	32,452,612
Testes	711,821 (86%)	1.43%	31,939,024
Liver	1,064,146 (84%)	1.84%	13,657,156
Medulla	380,531 (86%)	0.43%	48,256,918

Subcutaneous fat	215,759 (93%)	0.45%	42,043,313
Cerebral cortex	440,797 (87%)	1.01%	21,285,864
Jejunum	604,436 (90%)	2.331%	34,457,447

[1] Number in parentheses indicates mapping rate (90% coverage and 95% identity).

[2] In silco normalized using insilico_read_normalization.pl from Trinity (version 2.6.6) with the following settings: --max_cov 50 --max_pct_stdev 100 --single

Prediction of transcript and gene biotypes

Transcripts' open reading frames (ORFs) were predicted using the stand-alone version of ORFfinder (Wheeler et al. 2003) with "ATG and alternative initiation codons" as ORF start codon. The longest three ORFs were matched to the NCBI non-redundant vertebrate database and Uniprot vertebrate database using Blastp (Wheeler et al. 2003) with E-value cutoff of 10^{-6}, min coverage 60%, and min identity 95%. The ORFs with the lowest E-value to a protein were used as the representative, or if no matches were found, the longest ORF was used. Putative transcripts that had representative ORFs longer than 44 amino acids were labelled as protein-coding transcripts. If the representative ORF had a stop codon that was more than 50 bp upstream of the final splice junction, it was labelled as a nonsense-mediated decay transcript (Aken et al. 2016). Transcripts with start codon but no stop codon before their poly(A) site were labelled non-stop decay RNAs. Putative non-coding transcripts with lengths less than 200 bp were labelled as small non-coding RNAs (Aken et al. 2016). Putative non-coding transcripts with lengths greater than 200 bp were labelled as long non-coding RNAs (Aken et al. 2016). Long

non-coding RNAs overlapping one or more coding loci on the opposite strand were labelled as antisense lncRNAs. Long non-coding RNAs located in introns of coding genes on the same strand were labelled as sense-intronic lncRNAs. Long non-coding RNAs that exonically overlapped with a protein-coding gene were labeled as Intragenic lncRNAs. Long non-coding RNAs located in intergenic regions of the genome were labeled as Intergenic lncRNAs.

Putative genes that transcribed at least a single protein-coding transcript were labelled as protein-coding genes. Putative genes with homology to existing vertebrate protein-coding genes (Blastx (Wheeler et al. 2003), E-value cut-off 10^{-6}, min coverage 90%, and min identity 95%) but containing a disrupted coding sequence, i.e., transcribe only nonsense-mediated decay or non-stop decay transcripts in all of their detected tissues, were labelled as pseudogenes. The rest of the putative genes were labeled as non-coding.

Putative transcript structures were compared with independent bovine transcriptomes assembled from PacBio Iso-Seq data and RNA-seq data (see PacBio Iso-Seq data analysis), ONT-seq data (Halstead et al. 2021), and annotated transcripts from Ensembl (release 2021-03) and NCBI (Release 106) using Gffcompare (Pertea et al. 2016).

ncRNAs homology analysis

Non-coding RNAs were matched to NCBI and Ensembl vertebrate ncRNA databases using Blastn (Wheeler et al. 2003) with E-value cutoff of 10^{-6}, min coverage 90%, and min identity 95%.

Transcriptome termini site sequencing data analysis

T-rich stretches located at the 5′ end of each WTTS-seq raw read were removed using an in-house Perl script, as described previously (Zhou et al. 2016). T-trimmed reads were error-corrected using Coral (version 1.4.1) (Salmela and Schröder 2011) with -v -Y -u -a 3 option settings. The resulting reads were quality trimmed using FASTX Toolkit (version 0.0.14) (Hannon 2010) with -q 20 and -p 50 option settings. High-quality, error-corrected WTTS-seq reads were aligned against the ARS-UCD1.2 bovine genome using STAR (version 020201) (Dobin et al. 2013) with a cut-of of 95% identity and 90% coverage.

ChIP-seq and ATAC-seq data analysis

The UC Davis FAANG Functional Annotation Pipeline was applied to process the ChIP-seq and ATAC-seq data, as previously described (Kern et al. 2021). Briefly, the ARS-UCD1.2 genome assembly and Ensembl genome annotation (v100) were used as references for cattle. Sequencing reads were trimmed with Trim Galore! (Krueger et al. 2015) (v.0.6.5) and aligned with either STAR (Dobin et al. 2012) (v.2.5.4a) or BWA (Li et al. 2013) (v0.7.17) to the respective genome assemblies. Alignments with MAPQ scores <30 were filtered using Samtools (Li et la. 2009) (v.1.9). For ChIP-seq, after the filtering, duplicates were marked and removed using Picard (v.2.18.7). Regions of signal enrichment (“peaks”) were called by MACS2 (Zhang et al. 2008) (v.2.1.1).

Relating transcripts and genes to epigenetic data

The promoter was defined as the genomic region that spans from 500 bp 5′ to 100 bp 3′ of the gene/transcript start site. Histone mark or ATAC-seq (accesible chromatin) peaks mapped to the promoter of a given gene/transcript were related to that gene/transcript.

Transcript and gene border validation

RAMPAGE peaks from a previously published experiment (Goszczynski et al. 2021) were used to validate gene/transcript start site. Peaks within the genomic region that spans from 30 bp 5′ to 10 bp 3′ of a gene/transcript start site were assigned to that gene/transcript. WTTS-seq reads (median length of 161 nt) within the genomic region that spans from 10 bp 5′ to 165 bp 3′ of a gene/transcript terminal site were assigned to that gene/transcript.

Functional enrichment analysis

The potential mechanism of action of a group of genes was deciphered using ClueGO (Bindea et al. 2009). The latest update (May 2021) of the Gene Ontology Annotation database (GOA) (Huntley et al. 2015) was used in the analysis. The list of genes with at least one transcript detected in a given tissue was used as background for that tissue. The GO tree interval ranged from 3 to 20, with the minimum number of genes per cluster set to three. Term enrichment was tested with a right-sided hyper-geometric test that was corrected for multiple testing using the Benjamini-Hochberg procedure (Kim and van de Wiel 2008). The adjusted p-value threshold of 0.05 was used to filter enriched GO terms.

Alternative splicing analysis

Alternative splicing events, except Unique Splice Site Exons, were detected using generateEvents from SUPPA (version 2.3) (Trincado et al. 2018) with default settings. Unique Splice Site Exons were detected using an in-house Python script.

miRNA-seq data analysis

Single-end Qiagen miRNA-seq reads (50bp) from each tissue sample were trimmed to remove the adaptor sequences and low-quality bases using Trim Galore (version 0.6.4) (Krueger 2019) with --quality 20, --length 16, --max_length 30 -a AACTGTAGGCACCATCAAT option settings. miRNA reads were aligned against the ARS-UCD1.2 bovine genome using mapper.pl from mirDeep2 (version 0.1.3) (Friedländer et al. 2012) with -e -h -q -j -l 16 -o 40 -r 1 -m -v -n option settings. miRNA mature sequences along with their hairpin sequences for Bos taurus species were downloaded from miRbase (Kozomara et al. 2019). These sequences, along with the aligned miRNA reads, were used to quantify known miRNAs in each sample using miRDeep2.pl from mirDeep2 (version 0.1.3) (Friedländer et al. 2012) with -t bta -c -v 2 setting options. miRNA normalized Reads Per Million (RPM) were used to check sample similarities using hierarchical clustering and regression analysis of gene expression values (log2 based CPM), and outlier samples were detected and removed from downstream analysis. In order to predict the most comprehensive set of novel miRNAs, samples from different tissues were concatenated into a single file that were aligned against the ARS-UCD1.2 bovine genome using mapper.pl from mirDeep2 (version 0.1.3) (Friedländer et al. 2012) with the aforementioned settings. Aligned reads from the previous step were used, along with known miRNAs' mature sequences and

their hairpins, to predict novel miRNAs using miRDeep2.pl from mirDeep2 (version 0.1.3) (Friedländer et al. 2012) with the aforementioned settings. Samples from each tissue were combined to get the most comprehensive set of data for that tissue. Mature miRNA sequences and their hairpins for both known and predicted novel miRNAs' sequences along with the aligned miRNA reads from each tissue were used to quantify known and novel miRNAs in each tissue using mirDeep2 (version 0.1.3) (Friedländer et al. 2012) with the aforementioned settings.

Tissue-specificity index

Tissue Specificity Index (TSI) calculations were utilized to present more comprehensive information on transcript/gene/miRNA expression patterns across tissues. This index has a range of zero to one with a score of zero corresponding to ubiquitously expressed transcripts/genes/miRNAs (i.e., "housekeepers") and a score of one for transcripts/genes/miRNAs that are expressed in a single tissue (i.e., "tissue-specific") (Ludwig et al. 2016). The TSI for a transcript/gene/miRNA j was calculated as (Ludwig et al. 2016):

$$TSI_j = \frac{\sum_{i=1}^{N}\left(1 - x_{j,i}\right)}{N - 1}$$

where N corresponds to the total number of tissues measured, and $x_{j,i}$ is the expression intensity of tissue i normalized by the maximal expression of any tissue for transcript/gene/miRNA j.

QTL enrichment analysis

Publicly available bovine QTLs were retrieved from AnimalQTLdb (Hu et al. 2019). Genes closest to a given trait's QTLs were denoted as QTL-associated genes for that trait. The median distance of QTLs located outside gene borders to the closest gene was 51.9 kilobases and the maximum distance was 2.6 million bases. QTL enrichment was tested with a right-sided Fisher Exact test using an in-house Python script. The resulting p-values were corrected for multiple testing by the Benjamini-Hochberg procedure (Kim and van de Wiel 2008). The adjusted p-value threshold of 0.05 was used to filter QTLs.

Trait similarity network

For a given pair of traits, trait A was denoted as "similar" to trait B if a significant portion of trait A's QTL-associated genes were also the closest genes to trait B QTLs based on 1000 permutation tests. The resulting p-values were corrected for multiple testing using the Benjamini-Hochberg procedure (Kim and van de Wiel 2008). The same procedure was used to test trait B's similarity to trait A. The adjusted p-value threshold of 0.05 was used to filter significant trait similarities. A graphical presentation of the method used to construct the tissue similarity network is presented in Supplemental file 1: Fig. S39. The resulting network was visualized using Cystoscape software (Shannon et al. 2003).

Testis-pituitary axis correlation significance test

The presence of signal peptides on representative ORFs of protein-coding transcripts was predicted using SignalP-5.0 (Almagro Armenteros et al. 2019). Spearman correlation coefficients were used to study expression similarity between testis genes encoding signal peptides that were closest to the "percentage of normal sperm" QTLs (62 genes) and pituitary genes closest to the "percentage of normal sperm" QTLs (246 genes). To test the statistical difference between these correlation coefficients (reference correlations) and random chance, 1000 random sets of 246 pituitary genes were selected, and their correlation coefficients with 62 previously described testis genes were calculated (random correlations). The reference correlations were compared with 1000 sets of random correlations using a right-sided t-test. The resulting p-values were corrected for multiple testing by the Benjamini-Hochberg procedure (Kim and van de Wiel 2008). The distribution-adjusted p-values were used to determine the significance level of expression similarities for genes involved in the testis-pituitary axis related to "percentage of normal sperm". The same analysis was conducted to determine the significance of pituitary-testis axis involvement in this trait.

Tissue dendrogram comparison across different transcript and gene biotypes

Tissues were clustered based on the percentage of their transcripts/genes that were shared between tissue pairs using the hclust function in R. Cophenetic distances for tissue dendrograms were calculated using the cophenetic R function. The degree of similarity between dendrograms constructed based on different gene/transcript biotypes was obtained using the Spearman correlation coefficient between the dendrograms' Cophenetic distances.

Supplemental files

Supplemental file 1: Fig. S1 Distribution of the number of RNA-seq reads across tissues. **Fig. S2** (A) Comparison of tissues based on number of transcript biotypes and (B) percentage of transcript biotypes. (C) Comparison of transcript biotypes based on their number of detected tissues and (D) their expression level across detected tissues. **Fig. S3** (A) Relation between the number of input reads and the number of transcript biotypes (B) Comparison of expression level between different transcript biotypes. **Fig. S4** Tissue similarities (A) and clustering (B) based on the percentage of protein-coding transcripts shared between pairs of tissues. **Fig. S5** Tissue similarities (A) and clustering (B) based on the percentage of non-coding transcripts shared between pairs of tissues. **Fig. S6** Comparison of known and novel transcripts based on their expression (A) and number of detected tissues (B). **Fig. S7** Comparison of known and novel protein-coding transcripts based on the length (A) and GC content (B) of their 5' UTR, CDS, and 3' UTR. **Fig. S8** (A) Comparison of tissues based on number of gene biotypes and (B) percentage of gene biotypes. **Fig. S9** Relation between the number of input reads and the number of gene biotypes**. Fig. S10** Comparison of known and novel genes based on their expression (A) and number of detected tissues (B). **Fig. S11** Functional enrichment analysis of the top five percent of genes with the highest number of UTRs. **Fig. S12** Similarity of tissues based on the number of non-coding genes in their fetal samples that switched to protein-coding genes with only coding transcripts in their adult samples. **Fig. S13** (A) Distribution of genes that transcribed PATs, based on their number of detected tissues, percentage of genes' transcripts that are PATs and percentage of genes' detected tissues in which PATs were transcribed. (B) Comparison of genes that transcribed PATs with other gene biotypes. **Fig. S14** (A) Homology analysis of protein-

coding genes. (B) Homology analysis of non-coding genes. (C) Detection of orphan genes based on homology classification of cattle-specific protein-coding genes and non-coding genes. **Fig. S15** Comparison of the expression level of homologous and orphan genes across (A) and within (B) their detected tissues. (C) Comparison of homologous and orphan genes based on the number of detected tissues. **Fig. S16** Comparison of different gene biotypes based on the expression (A) and the number of detected tissues (B). **Fig. S17** Comparison of different pseudogene-derived lncRNAs and non-pseudogene derived lncRNAs based on the expression level (A) and the number of detected tissues (B)**. Fig. S18** Tissue similarities (A) and clustering (B) based on the percentage of protein-coding genes shared between pairs of tissues. **Fig. S19** Tissue similarities (A) and clustering (B) based on the percentage of non-coding genes shared between pairs of tissues. **Fig. S20** (A) Different types of alternative splicing events. (B) Comparison of bovine genome builds based on the number of transcripts that showed any type of alternative splicing (AS) events**. Fig. S21** Comparison of tissues based on the number (A) and the percentage (B) of transcripts that showed different types of alternative splicing events. Comparison of tissues based on the number (C) and the percentage (D) of alternative splicing events**. Fig. S22** (A) Comparison of tissues based on the percentage of transcripts that showed any type of alternative splicing events, spliced transcripts from single-transcript genes, and unspliced transcripts and (B) the relation between the number of input reads and the number of these transcripts across tissues. **Fig. S23** Comparison of transcripts that showed different types of alternative splicing events based on (A) the expression level in the detected tissues and (B) the number of detected tissues. **Fig. S24** Transcript biotype switching due to alternative splicing events**. Fig. S25** Comparison of tissues based on the number of alternative splicing

events per alternatively spliced gene**. Fig. S26** (A) Distribution of the number of alternative splicing events per alternatively spliced gene. The 5% quantile is shown using a dashed red line. (B) Functional enrichment analysis of the top five percent of genes with the highest number of alternative splicing events. **Fig. S27** Comparison of the alternative splicing rate between adult and fetal tissues. **Fig. S28** (A) Distribution of gene's number of detected tissues. Tissue-specific gene biotypes are shown in the pie chart. (B) Distribution of transcript's number of detected tissues. Tissue-specific transcript biotypes are shown in the pie chart. (C) Comparison of tissues based on the number of tissue-specific genes and transcripts. (D) Comparison of the expression level of tissue-specific genes and transcripts versus their non-tissue-specific counterparts. **Fig. S29** Relationship between tissue specificity and alternative splicing events**. Fig. S30** Relationship between tissue specificity index and the number of multi-tissue detected genes (A) and transcripts (B). Distribution of tissue specificity indexes in multi-tissue detected genes (C) and transcripts (D). The 5% quantile is shown using dashed red lines. (E) Functional enrichment analysis of the top five percent of multi-tissue detected genes with the highest tissue specificity indexes. **Fig. S31** Distribution of QTLs located outside gene borders in relation to the closest gene**. Fig. S32** (A) Distribution of correlation coefficients between SPACA5 gene expression and pituitary genes closest to "percentage of normal sperm" QTLs. Dashed lines show the minimum significant positive and negative correlation (p-value <0.05). (B) Expression atlas of SPACA5 gene in human tissues from The Human Protein Atlas (Uhlén et al. 2015). **Fig. S33** (A) Correlation between pituitary genes with signal peptides that were close to the "percentage of normal sperm" QTL and testis genes closest to this trait's QTL (reference correlations). (B) Distribution of p-values resulting from right-sided t-test between reference correlation

coefficients and correlation coefficients derived from random chance (see methods for details)**.** **Fig. S34** Tissue similarities (A) and clustering (B) based on the percentage of miRNAs shared between pairs of tissues. **Fig. S35** Clustering of tissues based on protein-coding genes (A), protein-coding transcripts (B), non-coding genes (C), non-coding transcripts (D), and miRNAs (E). (F) Comparison of tissue dendrograms based on the correlation between their Cophenetic distances. **Fig. S36** (A) Distribution of the number of detected tissues for known and novel miRNAs. Classification of miRNAs as known, or novel is presented in the pie chart. (B) Comparison of tissues based on their number of tissue-specific miRNAs. (C) Expression of known and novel miRNAs in their detected tissues. (D) Distribution of multi-tissue detected miRNAs' tissue specificity indexes. (E) Relationship between tissue specificity index and number of detected tissues in multi-tissue detected miRNAs. Dots have been color coded based on their density. **Fig. S37** Distribution of the number of detected genes (A), transcripts (B), and miRNAs (C) across tissues. **Fig. S38** Distribution of the number of known and novel genes (A), transcripts (B), and miRNAs (C) across tissues. **Fig. S39** Graphical representation of the method used to construct the tissue similarity network.

Supplemental file 2: Summary of RNA-seq and miRNA-seq reads

Supplemental file 3: Detailed description of the number of transcripts, genes, and miRNAs detected in each tissue

Supplemental file 4: List of transcripts and genes expressed in each tissue and their expression values (RPKM)

Supplemental file 5: Transcript biotype enrichment analysis in adult and fetal tissues

Supplemental file 6: Functional enrichment analysis of the top five percent of genes with the highest number of UTRs

Additional file7: Functional enrichment analysis of genes that remained bifunctional in all their detected tissues

Additional file8: Functional enrichment analysis of non-coding genes in fetal tissues that were switched to protein coding with only coding transcripts in their matched adult tissue

Additional file9: Functional enrichment analysis of protein-coding genes that transcribed PATs as their main transcripts (PATs comprised >50% of their transcripts) in all their detected tissues

Supplemental file 10: Gene biotype enrichment analysis in adult and fetal tissues

Supplemental file 11: Functional enrichment analysis of the top five percent of genes with the highest number of alternative splicing events

Additional file12: List of tissue-specific genes and transcripts

Additional file13: Genes and transcripts tissue specificity indexes

Additional file14: Functional enrichment analysis of the top five percent of multi-tissue detected genes with the highest tissue specificity indexes

Additional file15: List of QTL's closest genes in each tissue

Additional file16: Trait enrichment analysis of testis-specific genes

Additional file16: Pituitary genes closest to "percentage of normal sperm" QTLs that showed positive significant correlation with SPACA5 gene in testis

Additional file18: List of genes closest to "percentage of normal sperm" QTLs that were involved in testis-pituitary tissue axis and their functional enrichment analysis results

Additional file19: List of genes closest to "percentage of normal sperm" QTLs that were involved in pituitary-testis tissue axis and their functional enrichment analysis results

Additional file20: Similarity of traits based on the integration of the assembled bovine transcriptome with publicly available QTLs

Additional file21: List of miRNAs expressed in each tissue and their expression values

Additional file22: List of tissues related to different omics datasets used in the experiment

Data availability

RNA-seq and miRNA-seq, ATAC-seq, and WTTS-seq datasets generated in this study are submitted to the ArrayExpress database (https://www.ebi.ac.uk/arrayexpress/) under accession numbers MTAB-11699, E-MTAB-11815, and E-MTAB-12052, respectively. PacBio Iso-Seq, ChIP-seq, and RAMPAGE datasets generated in this study are submitted to the NCBI BioProject database (https://www.ncbi.nlm.nih.gov/bioproject/) under accession numbers PRJNA386670, GSE158416, and PRJNA630504, respectively. The constructed bovine trait similarity network is publicly available through the Animal Genome database (https://www.animalgenome.org/host/reecylab/a). The constructed cattle transcriptome and

related sequences are publicly available in the Open Science Framework database (https://osf.io/jze72/?view_only=d2dd1badf37e4bafae1e12731a0cc40d). Custom code used is available at https://github.com/hamidbeiki/Cattle-Genome.

Ethics approval and consent to participate

Procedures for tissue collection followed the Animal Care and Use protocol (#18464) approved by the Institutional Animal Care and Use Committee (IACUC), University of California, Davis (UCD).

Consent for publication

Not applicable

Competing interests

The authors declare no competing interests.

Funding

This study was supported by Agriculture and Food Research Initiative Competitive Grant no. 2018-67015-27500 (H.Z., P.R. etc.) and sample collection was supported by no. 2015-67015-22940 (H.Z. and P.R.) from the USDA National Institute of Food and Agriculture.

Acknowledgments

We are grateful to Nathan Weeks for helping with massive parallel computing of transcriptome assembly.

Authors' contributions

H.B., B.M.M., H.J., H.Z., M.R., P.J.R., S.M., T.P.L.S., W.L., Z.J., and J.M.R. conceived and designed the project; C.K., W.M., and W.L. generated RNA-seq and miRNA-seq data; D.K., G.B., J.T., and K.D. participated in tissue collection; R.H and H.J prepared cells; J.J.M., X.Z., X.H., and Z.J. generated W.T.T.S-seq data, X.X., P.J.R. and H.J generated ChIP-seq data; M.R.J. generated ATAC-seq data; T.P.L.S. generated PacBio Iso-seq data; G.R. and S.C. conducted sequencing of RNA-seg, miRNA-seq, ChIP-seq, and ATAC-seq data; H.B. conducted bioinformatics data analysis and drafted the manuscript, which was edited by C.A.P., B.M.M., H.J., H.Z., J.E.K., M.R., P.J.R., S.M., T.P.L.S., W.L., Z.J. and J.M.R.; Z.H. created the web-based database for the trait similarity network; all authors read and approved the final manuscript.

Endnotes

Mention of trade names or commercial products in this publication is solely for the purpose of providing specific information and does not imply recommendation or endorsement by the U.S. Department of Agriculture. USDA is an equal opportunity provider and employer.

The results reported here were made possible with resources provided by the USDA shared computing cluster (Ceres) as part of the ARS SCINet initiative.

References

Aken BL, Ayling S, Barrell D, Clarke L, Curwen V, Fairley S, Fernandez Banet J, Billis K, García Girón C, Hourlier T et al. 2016. The Ensembl gene annotation system. *Database (Oxford)* **2016**.

Almagro Armenteros JJ, Tsirigos KD, Sønderby CK, Petersen TN, Winther O, Brunak S, von Heijne G, Nielsen H. 2019. SignalP 5.0 improves signal peptide predictions using deep neural networks. *Nature Biotechnology* **37**: 420-423.

Ambros V. 2004. The functions of animal microRNAs. *Nature* **431**: 350-355.

Anderson DM, Anderson KM, Chang CL, Makarewich CA, Nelson BR, McAnally JR, Kasaragod P, Shelton JM, Liou J, Bassel-Duby R et al. 2015. A micropeptide encoded by a putative long noncoding RNA regulates muscle performance. *Cell* **160**: 595-606.

Andrews SJ, Rothnagel JA. 2014. Emerging evidence for functional peptides encoded by short open reading frames. *Nat Rev Genet* **15**: 193-204.

Araujo PR, Yoon K, Ko D, Smith AD, Qiao M, Suresh U, Burns SC, Penalva LO. 2012. Before It Gets Started: Regulating Translation at the 5' UTR. *Comp Funct Genomics* **2012**: 475731.

Bartel DP. 2004. MicroRNAs: genomics, biogenesis, mechanism, and function. *Cell* **116**: 281-297.

Beiki H, Liu H, Huang J, Manchanda N, Nonneman D, Smith TPL, Reecy JM, Tuggle CK. 2019. Improved annotation of the domestic pig genome through integration of Iso-Seq and RNA-seq data. *BMC Genomics* **20**: 344.

1253 Bindea G, Mlecnik B, Hackl H, Charoentong P, Tosolini M, Kirilovsky A, Fridman WH, Pagès F,
1254 Trajanoski Z, Galon J. 2009. ClueGO: a Cytoscape plug-in to decipher functionally
1255 grouped gene ontology and pathway annotation networks. *Bioinformatics* **25**: 1091-
1256 1093.

1257 Chen J, Chen ZJ. 2013. Regulation of NF-κB by ubiquitination. *Curr Opin Immunol* **25**: 4-12.

1258 Clare M, Richard P, Kate K, Sinead W, Mark M, David K. 2018. Residual feed intake phenotype
1259 and gender affect the expression of key genes of the lipogenesis pathway in
1260 subcutaneous adipose tissue of beef cattle. *J Anim Sci Biotechnol* **9**: 68.

1261 Colombo M, Karousis ED, Bourquin J, Bruggmann R, Mühlemann O. 2017. Transcriptome-wide
1262 identification of NMD-targeted human mRNAs reveals extensive redundancy between
1263 SMG6- and SMG7-mediated degradation pathways. *RNA* **23**: 189-201.

1264 Dobin A, Davis CA, Schlesinger F, Drenkow J, Zaleski C, Jha S, Batut P, Chaisson M, Gingeras TR.
1265 2013. STAR: ultrafast universal RNA-seq aligner. *Bioinformatics* **29**: 15-21.

1266 Elolimy AA, Abdelmegeid MK, McCann JC, Shike DW, Loor JJ. 2018. Residual feed intake in beef
1267 cattle and its association with carcass traits, ruminal solid-fraction bacteria, and
1268 epithelium gene expression. *J Anim Sci Biotechnol* **9**: 67.

1269 Farr VC, Stelwagen K, Cate LR, Molenaar AJ, McFadden TB, Davis SR. 1996. An improved method
1270 for the routine biopsy of bovine mammary tissue. *J Dairy Sci* **79**: 543-549.

1271 Friedländer MR, Mackowiak SD, Li N, Chen W, Rajewsky N. 2012. miRDeep2 accurately
1272 identifies known and hundreds of novel microRNA genes in seven animal clades. *Nucleic*
1273 *Acids Res* **40**: 37-52.

1274 Gerber S, Schratt G, Germain PL. 2021. Streamlining differential exon and 3' UTR usage with
1275 diffUTR. *BMC Bioinformatics* **22**: 189.

1276 Gonzàlez-Porta M, Frankish A, Rung J, Harrow J, Brazma A. 2013. Transcriptome analysis of
1277 human tissues and cell lines reveals one dominant transcript per gene. *Genome Biol* **14**:
1278 R70.

1279 Goszczynski DE, Halstead MM, Islas-Trejo AD, Zhou H, Ross PJ. 2021. Transcription initiation
1280 mapping in 31 bovine tissues reveals complex promoter activity, pervasive transcription,
1281 and tissue-specific promoter usage. *Genome Res* **31**: 732-744.

1282 Grabherr MG, Haas BJ, Yassour M, Levin JZ, Thompson DA, Amit I, Adiconis X, Fan L,
1283 Raychowdhury R, Zeng Q et al. 2011. Full-length transcriptome assembly from RNA-Seq
1284 data without a reference genome. *Nat Biotechnol* **29**: 644-652.

1285 Green TC, Jago JG, Macdonald KA, Waghorn GC. 2013. Relationships between residual feed
1286 intake, average daily gain, and feeding behavior in growing dairy heifers. *J Dairy Sci* **96**:
1287 3098-3107.

1288 Hackl T, Hedrich R, Schultz J, Förster F. 2014. proovread: large-scale high-accuracy PacBio
1289 correction through iterative short read consensus. *Bioinformatics* **30**: 3004-3011.

1290 Halasa T, Kirkeby C. 2020. Differential Somatic Cell Count: Value for Udder Health Management.
1291 *Front Vet Sci* **7**: 609055.

1292 Halstead MM, Islas-Trejo A, Goszczynski DE, Medrano JF, Zhou H, Ross PJ. 2021. Large-Scale
1293 Multiplexing Permits Full-Length Transcriptome Annotation of 32 Bovine Tissues From a
1294 Single Nanopore Flow Cell. *Front Genet* **12**: 664260.

1295 Hannon GJ. 2010. FASTX-Toolkit. http://hannonlab.cshl.edu/fastx_toolkit.

1296 Hass B. 2015. https://hpcgridrunner.github.io/.

1297 Hertl JA, Schukken YH, Tauer LW, Welcome FL, Gröhn YT. 2018. Does clinical mastitis in the first
1298 100 days of lactation 1 predict increased mastitis occurrence and shorter herd life in
1299 dairy cows? *J Dairy Sci* **101**: 2309-2323.

1300 Hindorff LA, Sethupathy P, Junkins HA, Ramos EM, Mehta JP, Collins FS, Manolio TA. 2009.
1301 Potential etiologic and functional implications of genome-wide association loci for
1302 human diseases and traits. *Proc Natl Acad Sci U S A* **106**: 9362-9367.

1303 Houlahan K, Schenkel FS, Hailemariam D, Lassen J, Kargo M, Cole JB, Connor EE, Wegmann S,
1304 Junior O, Miglior F et al. 2021. Effects of Incorporating Dry Matter Intake and Residual
1305 Feed Intake into a Selection Index for Dairy Cattle Using Deterministic Modeling.
1306 *Animals (Basel)* **11**.

1307 Hu ZL, Park CA, Reecy JM. 2019. Building a livestock genetic and genomic information
1308 knowledgebase through integrative developments of Animal QTLdb and CorrDB. *Nucleic*
1309 *Acids Res* **47**: D701-D710.

1310 Hubé F, Velasco G, Rollin J, Furling D, Francastel C. 2011. Steroid receptor RNA activator protein
1311 binds to and counteracts SRA RNA-mediated activation of MyoD and muscle
1312 differentiation. *Nucleic Acids Res* **39**: 513-525.

1313 Huntley RP, Sawford T, Mutowo-Meullenet P, Shypitsyna A, Bonilla C, Martin MJ, O'Donovan C.
1314 2015. The GOA database: gene Ontology annotation updates for 2015. *Nucleic Acids Res*
1315 **43**: D1057-1063.

1316 Jereb S, Hwang HW, Van Otterloo E, Govek EE, Fak JJ, Yuan Y, Hatten ME, Darnell RB. 2018.
1317 Differential 3' Processing of Specific Transcripts Expands Regulatory and Protein
1318 Diversity Across Neuronal Cell Types. *Elife* **7**.

1319 Kaniyamattam K, De Vries A, Tauer LW, Gröhn YT. 2020. Economics of reducing antibiotic usage
1320 for clinical mastitis and metritis through genomic selection. *J Dairy Sci* **103**: 473-491.

1321 Karalis KP, Venihaki M, Zhao J, van Vlerken LE, Chandras C. 2004. NF-kappaB participates in the
1322 corticotropin-releasing, hormone-induced regulation of the pituitary
1323 proopiomelanocortin gene. *J Biol Chem* **279**: 10837-10840.

1324 Kern C, Wang Y, Xu X, Pan Z, Halstead M, Chanthavixay G, Saelao P, Waters S, Xiang R,
1325 Chamberlain A et al. 2021. Functional annotations of three domestic animal genomes
1326 provide vital resources for comparative and agricultural research. *Nat Commun* **12**:
1327 1821.

1328 Kim KI, van de Wiel MA. 2008. Effects of dependence in high-dimensional multiple testing
1329 problems. *BMC Bioinformatics* **9**: 114.

1330 Kozomara A, Birgaoanu M, Griffiths-Jones S. 2019. miRBase: from microRNA sequences to
1331 function. *Nucleic Acids Res* **47**: D155-D162.

1332 Krueger F. 2019. https://www.bioinformatics.babraham.ac.uk/projects/trim_galore/.

1333 Kumar S, Lee HJ, Park HS, Lee K. 2016. Testis-Specific GTPase (TSG): An oligomeric protein. *BMC*
1334 *Genomics* **17**: 792.

1335 Kumari P, Sampath K. 2015. cncRNAs: Bi-functional RNAs with protein coding and non-coding
1336 functions. *Semin Cell Dev Biol* **47-48**: 40-51.

1337 Kurosaki T, Popp MW, Maquat LE. 2019. Quality and quantity control of gene expression by
1338 nonsense-mediated mRNA decay. *Nat Rev Mol Cell Biol* **20**: 406-420.

1339 Leek J, Johnson W, Parker HS, Fertig EJ, Jaffe AE, Zhang Y, Storey JD, LC T. 2021. *sva: Surrogate*
1340 *Variable Analysis* . R package version 3.30.0.

1341 Li J, Liu C. 2019. Coding or Noncoding, the Converging Concepts of RNAs. *Front Genet* **10**: 496.

1342 Liao Y, Smyth GK, Shi W. 2014. featureCounts: an efficient general purpose program for
1343 assigning sequence reads to genomic features. *Bioinformatics* **30**: 923-930.

1344 Lima FS, Silvestre FT, Peñagaricano F, Thatcher WW. 2020. Early genomic prediction of daughter
1345 pregnancy rate is associated with improved reproductive performance in Holstein dairy
1346 cows. *J Dairy Sci* **103**: 3312-3324.

1347 Liu E, VandeHaar MJ. 2020. Relationship of residual feed intake and protein efficiency in
1348 lactating cows fed high- or low-protein diets. *J Dairy Sci* **103**: 3177-3190.

1349 Lou W, Ding B, Fu P. 2020. Pseudogene-Derived lncRNAs and Their miRNA Sponging Mechanism
1350 in Human Cancer. *Front Cell Dev Biol* **8**: 85.

1351 Ludwig N, Leidinger P, Becker K, Backes C, Fehlmann T, Pallasch C, Rheinheimer S, Meder B,
1352 Stähler C, Meese E et al. 2016. Distribution of miRNA expression across human tissues.
1353 *Nucleic Acids Res* **44**: 3865-3877.

1354 Mackowiak SD, Zauber H, Bielow C, Thiel D, Kutz K, Calviello L, Mastrobuoni G, Rajewsky N,
1355 Kempa S, Selbach M et al. 2015. Extensive identification and analysis of conserved small
1356 ORFs in animals. *Genome Biol* **16**: 179.

1357 Martí De Olives A, Díaz JR, Molina MP, Peris C. 2013. Quantification of milk yield and
1358 composition changes as affected by subclinical mastitis during the current lactation in
1359 sheep. *J Dairy Sci* **96**: 7698-7708.

1360 Mayba O, Gilbert HN, Liu J, Haverty PM, Jhunjhunwala S, Jiang Z, Watanabe C, Zhang Z. 2014.
1361 MBASED: allele-specific expression detection in cancer tissues and cell lines. *Genome*
1362 *Biol* **15**: 405.

1363 Mazin PV, Khaitovich P, Cardoso-Moreira M, Kaessmann H. 2021. Alternative splicing during
1364 mammalian organ development. *Nature Genetics* **53**: 925-934.

1365 Miles AM, McArt JAA, Leal Yepes FA, Stambuk CR, Virkler PD, Huson HJ. 2019. Udder and teat
1366 conformational risk factors for elevated somatic cell count and clinical mastitis in New
1367 York Holsteins. *Prev Vet Med* **163**: 7-13.

1368 Milligan MJ, Lipovich L. 2014. Pseudogene-derived lncRNAs: emerging regulators of gene
1369 expression. *Front Genet* **5**: 476.

1370 Mitrovich QM, Anderson P. 2005. mRNA surveillance of expressed pseudogenes in C. elegans.
1371 *Curr Biol* **15**: 963-967.

1372 Nam JW, Choi SW, You BH. 2016. Incredible RNA: Dual Functions of Coding and Noncoding. *Mol*
1373 *Cells* **39**: 367-374.

1374 Nickless A, Bailis JM, You Z. 2017. Control of gene expression through the nonsense-mediated
1375 RNA decay pathway. *Cell Biosci* **7**: 26.

1376 O'Shaughnessy PJ, Fleming LM, Jackson G, Hochgeschwender U, Reed P, Baker PJ. 2003.
1377 Adrenocorticotropic hormone directly stimulates testosterone production by the fetal
1378 and neonatal mouse testis. *Endocrinology* **144**: 3279-3284.

1379 Olexiouk V, Crappé J, Verbruggen S, Verhegen K, Martens L, Menschaert G. 2016. sORFs.org: a
1380 repository of small ORFs identified by ribosome profiling. *Nucleic Acids Res* **44**: D324-
1381 329.

1382 PacificBiosciences. 2018. https://www.pacb.com/products-and-services/analytical-
1383 software/smrt-analysis/.

1384 Pedersen BS, Quinlan AR. 2018. Mosdepth: quick coverage calculation for genomes and
1385 exomes. *Bioinformatics* **34**: 867-868.

1386 Pertea M, Kim D, Pertea GM, Leek JT, Salzberg SL. 2016. Transcript-level expression analysis of
1387 RNA-seq experiments with HISAT, StringTie and Ballgown. *Nat Protoc* **11**: 1650-1667.

1388 Rajala-Schultz PJ, Gröhn YT, McCulloch CE, Guard CL. 1999. Effects of clinical mastitis on milk
1389 yield in dairy cows. *J Dairy Sci* **82**: 1213-1220.

1390 Remnant J, Green MJ, Huxley J, Hirst-Beecham J, Jones R, Roberts G, Hudson CD. 2019.
1391 Association of lameness and mastitis with return-to-service oestrus detection in the
1392 dairy cow. *Vet Rec* **185**: 442.

1393 Richburg JH, Myers JL, Bratton SB. 2014. The role of E3 ligases in the ubiquitin-dependent
1394 regulation of spermatogenesis. *Semin Cell Dev Biol* **30**: 27-35.

1395 Roth JA, Tuggle CK. 2015. Livestock models in translational medicine. *ILAR J* **56**: 1-6.

1396 Salmela L, Schröder J. 2011. Correcting errors in short reads by multiple alignments.
1397 *Bioinformatics* **27**: 1455-1461.

1398 Sammeth M, Foissac S, Guigó R. 2008. A general definition and nomenclature for alternative
1399 splicing events. *PLoS Comput Biol* **4**: e1000147.

1400 Schurch NJ, Cole C, Sherstnev A, Song J, Duc C, Storey KG, McLean WH, Brown SJ, Simpson GG,
1401 Barton GJ. 2014. Improved annotation of 3' untranslated regions and complex loci by
1402 combination of strand-specific direct RNA sequencing, RNA-Seq and ESTs. *PLoS One* **9**:
1403 e94270.

1404 Shannon P, Markiel A, Ozier O, Baliga NS, Wang JT, Ramage D, Amin N, Schwikowski B, Ideker T.
1405 2003. Cytoscape: a software environment for integrated models of biomolecular
1406 interaction networks. *Genome Res* **13**: 2498-2504.

1407 Stewart GL, Enfield KSS, Sage AP, Martinez VD, Minatel BC, Pewarchuk ME, Marshall EA, Lam
1408 WL. 2019. Aberrant Expression of Pseudogene-Derived lncRNAs as an Alternative
1409 Mechanism of Cancer Gene Regulation in Lung Adenocarcinoma. *Front Genet* **10**: 138.

1410 Supek F, Lehner B, Lindeboom RGH. 2021. To NMD or Not To NMD: Nonsense-Mediated mRNA
1411 Decay in Cancer and Other Genetic Diseases. *Trends Genet* **37**: 657-668.

1412 Tange O. 2018. GNU Parallel. https://doi.org/10.5281/zenodo.1146014.

1413 Tixier-Boichard M, Fabre S, Dhorne-Pollet S, Goubil A, Acloque H, Vincent-Naulleau S, Ross P,
1414 Wang Y, Chanthavixay G, Cheng H et al. 2021. Tissue Resources for the Functional
1415 Annotation of Animal Genomes. *Front Genet* **12**: 666265.

1416 Trincado JL, Entizne JC, Hysenaj G, Singh B, Skalic M, Elliott DJ, Eyras E. 2018. SUPPA2: fast,
1417 accurate, and uncertainty-aware differential splicing analysis across multiple conditions.
1418 *Genome Biol* **19**: 40.

1419 Uhlén M, Fagerberg L, Hallström BM, Lindskog C, Oksvold P, Mardinoglu A, Sivertsson Å, Kampf
1420 C, Sjöstedt E, Asplund A et al. 2015. Proteomics. Tissue-based map of the human
1421 proteome. *Science* **347**: 1260419.

1422 Wang JR, Holt J, McMillan L, Jones CD. 2018. FMLRC: Hybrid long read error correction using an
1423 FM-index. *BMC Bioinformatics* **19**: 50.

1424 Weber C, Hametner C, Tuchscherer A, Losand B, Kanitz E, Otten W, Singh SP, Bruckmaier RM,
1425 Becker F, Kanitz W et al. 2013. Variation in fat mobilization during early lactation

differently affects feed intake, body condition, and lipid and glucose metabolism in high-yielding dairy cows. *J Dairy Sci* **96**: 165-180.

Wei L-H, Guo JU. 2020. Coding functions of "noncoding" RNAs. *Science* **367**: 1074-1075.

Wheeler DL, Church DM, Federhen S, Lash AE, Madden TL, Pontius JU, Schuler GD, Schriml LM, Sequeira E, Tatusova TA et al. 2003. Database resources of the National Center for Biotechnology. *Nucleic Acids Res* **31**: 28-33.

Wollerton MC, Gooding C, Wagner EJ, Garcia-Blanco MA, Smith CW. 2004. Autoregulation of polypyrimidine tract binding protein by alternative splicing leading to nonsense-mediated decay. *Mol Cell* **13**: 91-100.

Yates LA, Norbury CJ, Gilbert RJ. 2013. The long and short of microRNA. *Cell* **153**: 516-519.

Yi Z, Li X, Luo W, Xu Z, Ji C, Zhang Y, Nie Q, Zhang D, Zhang X. 2018. Feed conversion ratio, residual feed intake and cholecystokinin type A receptor gene polymorphisms are associated with feed intake and average daily gain in a Chinese local chicken population. *J Anim Sci Biotechnol* **9**: 50.

Zhou X, Li R, Michal JJ, Wu XL, Liu Z, Zhao H, Xia Y, Du W, Wildung MR, Pouchnik DJ et al. 2016. Accurate Profiling of Gene Expression and Alternative Polyadenylation with Whole Transcriptome Termini Site Sequencing (WTTS-Seq). *Genetics* **203**: 683-697.